Experiments and Numerical Simulations of the Dynamics of an R.O.V. Thruster During Maneuvering

by

James H. Knowles

B.S., Mechanical Engineering
University of New Hampshire, 1994

B.Arch., Architecture
University of Idaho, 1981

Submitted to the Department of Ocean Engineering
in Partial Fulfillment of the Requirements for the Degree of

Master of Science in Ocean Engineering

at the

Massachusetts Institute of Technology

and the

Woods Hole Oceanographic Institution

September 1996

Signature of Author:.....
MIT/WHOI Joint Program in Applied Ocean Science and Engineering
August 9, 1996

Certified by:.....
Dr. Mark A. Grosenbaugh
Woods Hole Oceanographic Institution
Thesis Supervisor

Accepted by:.....
Professor Henrik Schmidt, Chairman
Joint Committee for Oceanographic Engineering
Massachusetts Institute of Technology
Woods Hole Oceanographic Institution

Experiments and Numerical Simulations of the Dynamics of an R.O.V. Thruster During Maneuvering

by

James H. Knowles

Submitted to the Department of Ocean Engineering on August 9, 1996 in partial fulfillment of the requirements for the Degree of Master of Science in Ocean Engineering

ABSTRACT

Propeller dynamics have typically been ignored in controller design, lumped into the category of 'unmodeled dynamics.' This is acceptable for propellers operating at constant speed in relatively uniform flows. Operational parameters of small remotely operated vehicles and autonomous underwater vehicles require a great deal of transient operation of the propellers. This and the small mass of the vehicles make the dynamics of the propellers a significant factor in vehicle control. Expanding roles of these vehicles require improved control and therefore improved understanding of the dynamics of the thrusters during maneuvering.

In this thesis, the dynamics of maneuvering thrusters were explored through numerical simulation and experiments. Vortex lattice propeller code developed for use with nonuniform inflow was adapted to incorporate varying propeller speed and inflow velocity. Test runs were made using a three bladed propeller. Experiments were preformed on a thruster from the ROV *Jason* using the water tunnel at the Massachusetts Institute of Technology. The thruster incorporated a ducted three bladed propeller. Runs were made using step changes in shaft velocity as well as sinusoidal perturbations on top of steady state velocities. Runs were also made incorporating fully reversing propeller operation. Experiments were done with and without the duct in place.

The numerical simulation and experimental results showed that accelerating propeller angular velocity created higher thrust values than steady state propeller operation at the corresponding instantaneous shaft velocity. Decelerating angular velocities created lower thrust values. This is attributed to a lag in the local flow velocity due to the momentum of the fluid. For the case of the accelerating propeller, the angle of attack at the blade is higher, resulting in higher lift force and greater thrust. Errors in the numerical code at low advance coefficients prevented direct comparison of numerical code results to experimental results.

Thesis Supervisor: Dr. Mark A. Grosenbaugh
Woods Hole Oceanographic Institution

Contents

Chapter I Introduction

1.1 Motivation

The latter half of this century has seen rapid expansion in use of remotely operated vehicles (ROV) and Autonomous Underwater Vehicles (AUV). Driven by the oil industry, oceanographic exploration and national defense, extensive development of vehicles now permits humanity to explore and work in the deep oceans without endangering humans by subjecting them to the hostile deep-water environment. These vehicles have depended almost exclusively on marine propellers for propulsion.

The vehicles are used in a wide range of operating environments. Vehicles are currently used everywhere from shallow water in coastal areas to mid-ocean regions over 4000 m deep. The latitude of operation ranges from the equatorial regions to work under ice above the arctic circle. They are also used in a wide range of operations, frequently on the same mission. It would not be unheard of for a vehicle to be used in a cruising mode to map a large area with side-scan sonar at a constant speed of one knot, then to be used to photograph features found with sonar or collect samples in a particular area. If these features are extremely delicate or the water is murky (requiring close-in photography), the vehicle may be required to perform finely controlled maneuvers, placing very high demands on the skill of the pilot and the vehicle control algorithm.

The maneuvering operations these vehicles are subjected to have

introduced new problems for control systems. Previous control systems for propeller operations treated propellers driven by electric motors as actuators which would deliver a given amount of thrust for a given amount of applied torque [1]. The transient behavior of propulsors undergoing changes in angular velocity was lumped into the category of unmodeled dynamics and dealt with by applying robust control algorithms. This could be done for most propeller applications since the extreme mass of the vehicles involved and the relative time of unsteady operation compared to steady operation made the slight variations of thrust insignificant.

This is not the case with ROV's. Many of these vehicles are comparatively light. For example, the Woods Hole Oceanographic Institution's vehicle *Jason* is 1200 kg. More importantly, some operations require the vehicle's propulsor to operate exclusively within the transient regime. Hovering can require continual changes in propulsor angular velocity in order to maintain position, particularly in the presence of surge. Attempts to treat unsteady propeller dynamics as unmodeled disturbances has resulted in poor behavior, as noted by Whitcomb and Yoerger [2], Healy et al [3] and others.

Theories of propeller analysis and design used today have their roots in theories developed at the turn of the century. Ever powerful computers permit modeling of propellers today that include such difficult to define phenomena as cavitation and tip vortex roll-up. Almost all of this work has focused on optimizing propeller design centered on one ideal operating condition consisting of a fixed ship velocity, a constant propeller angular velocity and a constant distance below the free surface. This knowledge and experience has

been all that was available for designing ROV propellers that run at a wide variety of speeds, at constantly varying rpm and that frequently reverse direction. The result is that the vehicles are not meeting their full potential.

1.2 Objectives

The objective of this thesis is to provide background for the development of more accurate control algorithms in an effort to enable improved vehicle operations and to provide insight into the directions possible for improving thruster design. To accomplish this, a study was undertaken into the transient operation of an ROV thruster. Experiments were performed on an ROV thruster to gain a qualitative understanding of the thruster behavior under a variety of transient conditions. Data were taken that show qualitative differences in thrust between quasi-steady predictions and actual unsteady transient operations.

In addition, a numerical simulation used for predicting steady state behavior of a propeller was adapted to incorporate transient modes of operation. This tool should be useful in predicting transient behavior of propellers as well as for computer modeling of thruster dynamics.

Chapter II Propeller Theory

2.1 Development of Propeller Theory

The action of propellers has been understood at a basic level for some time. The basic principle follows Newton's laws, in which the propeller can be seen to be imparting a force on the fluid, resulting in an equal and opposite reaction of a fluid force on the propeller. A more rigorous development of propeller theory didn't get a sound start until the end of the 19th century with the development of the momentum theory. This development came from treatment of the propulsor as a jump in pressure in the fluid at the propeller, without concern for how this pressure jump occurred. Early work in this area is attributed to Rankine, Greenhill and Froude [4]. The classic approach is the actuator disk, first presented by Rankine.

The major contribution of the momentum theory was the definition of the maximum efficiency of an ideal propeller; it defined the upper limit of operation that could be expected of any propeller under a particular loading condition. It's major drawback is that it does not concern itself with the propeller itself. It is not interested in how the pressure jump is created. It does not even assume the presence of a propeller, so performance is not affected by propeller geometry.

A second theory that evolved at almost the same time was the blade element theory. In this case, the propeller's geometry was paramount. The forces acting on a blade were evaluated at several

locations and then integrated over the entire surface. This provided a means for evaluating different designs. It gave the incorrect result, however, that it was theoretically possible to have a propeller efficiency of one.

The two theories were resolved with the introduction of circulation. This was developed by F.W. Lanchester in 1907 for aerodynamic research, then applied to marine propellers by Betz and Prandtl. It can be shown that applying blade element theory with circulation to multi-blade propellers approaches the solution obtained from the actuator disk solution as the number of blades is increased. This culminates in the two solutions matching when the blade element theory is applied to an infinitely blade propeller [5].

2.2 Relevant Equations for Steady State Operations

The thrust expected from a propeller is a function of several quantities, including the blade geometry (span, chord, skew, rake, camber, thickness) and operating conditions. For a given propeller geometry, the thrust T from a propeller is proportional to the square of the angular velocity, Ω, or

$$T = C_1 \Omega |\Omega| \qquad (1)$$

where C_1 is a constant of proportionality dependent on the propeller and the fluid. This relationship assumes that the fluid is of constant density (ie: no cavitation).

The price of thrust is the torque required to turn the propeller. This is also a function of blade geometry and operating conditions. These two quantities are related to each other by the propeller's

efficiency [6], defined by

$$\eta = \frac{TV}{2\pi nQ} \tag{2}$$

where V is the velocity of the propeller through the water, n is the propeller angular velocity in revolutions per second, and Q is the torque.

2.3 Propeller Similitude

Three non-dimensional quantities are used frequently in propeller analysis and design. The first is the advance coefficient

$$J = \frac{V}{nD} \tag{3}$$

where D is the propeller diameter. The advance coefficient is a ratio of the speed of advance to the tangential velocity of the blade tip.

The forces involved are nondimensionalized using the density of the fluid ρ, the propeller speed of rotation n, and the propeller diameter D. The thrust coefficient K_t is

$$K_T = \frac{T}{\rho n^2 D^4} \tag{4}$$

and the torque coefficient K_q is

$$K_Q = \frac{Q}{\rho n^2 D^5} \tag{5}$$

Equations (3-5) are related to each other through the propeller efficiency (in open water)

$$\eta_o = \frac{J}{2\pi} x \frac{K_T}{K_Q} \tag{6}$$

Propeller data is most frequently presented by plotting K_t, $10xK_q$

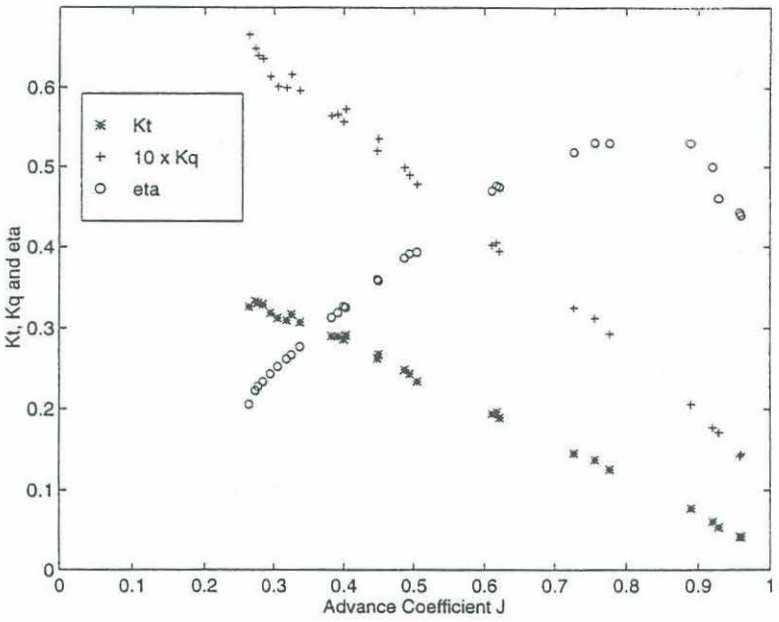

Figure 1: K_t and K_q curves for a three bladed propeller.

and η versus the advance coefficient. The values used are the ones obtained from open water tests. These values correspond to propellers operating in uniform flow without the effect of hull shapes upstream of the propeller. An example of this is shown in figure 1. This set of K_t K_q curves is for the three bladed Vetus propeller used in the experiments described in chapter five. To obtain these curves, the propeller was mounted to the shaft in the water tunnel at the hydrodynamics laboratory at the Massachusetts Institute of Technology. The duct used in conjunction with the propeller on the ROV *Jason* was also mounted to the shaft, but in such a way that the thrust provided by the duct was not included in the measurements. The facility, described in section 5.1, allowed for variations in both propeller angular velocity and inflow velocity, permitting for a wide variety of advance coefficients (equation (3)). Thrust and torque were recorded for several different J values, generating the plot.

One of the key points to be obtained from the K_t K_q curves is the ideal operating point of the propeller. This point is taken to be just prior of the point of maximum efficiency, allowing for slightly higher J values without severe drop-offs in efficiency. In the case of the propeller used to obtain figure 1, an operating point of 0.8 would be appropriate. This value gives an indication of the relationship of angular velocity and ship velocity that will result in optimum operation of the propeller.

Chapter III Numerical Simulation of Propellers

3.1 Use of Computers in Propeller Design

The development of the computer provided the ability to make substantial gains in the design and analysis of propellers. Computers allowed for the analysis of nontraditional blade shapes, including highly skewed blades to reduce vibration. In addition, they permitted the analysis of propellers in nonuniform inflows, caused by hull shape and shaft angle for example. This permitted better analysis of blade loading and consequently blade , shaft, and bearing stresses. This information was not available with systematic series data [7] [8].

Early use of computers in propeller design includes an elementary lifting line procedure developed by Kerwin in 1959. Three dimensional lifting surface theory for unsteady propeller was developed in the late 1960's. A summation of lifting surface theory development, as well as a thorough description of the methodology used at MIT is given in Kerwin and Lee [9].

3.2 Vortex Lattice Method

In the 1980's, lifting surface methods evolved into the vortex lattice method. These were more computationally efficient and more accurate, providing that local pressure distributions were not critical (for example, if cavitation inception was not important.) This was thoroughly introduced in Keenan [10]. The basics of this

method are outlined here.

In the Vortex Lattice Method, the propeller blades and wake are discretized through the use of straight line vortex elements. Each vortex element has a constant strength over it's length in accordance with Kelvin's Theorem. This requirement states that vorticity is constant and can only terminate at a surface or onto itself. The end points of the elements are connected to form a continuous lattice.

At the propeller blades, the end points of the elements are located at the mean camber surface of the blade. The elements are arranged so as to form a grid of panels. A 6 x 6 paneling of the blade is typical for simple blade shapes. The elements are spaced using cosine spacing. A control point is located at the geometric center of each panel, as shown in figure 2. The boundary value problem states that there is no flow through the blade at the control points, or

$$\overline{V} \bullet \overline{n} = 0 \tag{7}$$

in a blade fixed coordinate system, where **V** is the inflow, and **n** is the normal to the blade.

The trailing edge elements are located beyond the geometric trailing edge of the blade, along an extension of the blade's camber surface. These are coincident with the first row of vortex elements which represent the wake. The location of these elements, $\mathbf{x}_{w1}$, relative to the trailing edge of the blade, $\mathbf{x}_{te}$, is given by the equation

$$\boldsymbol{x}_{w_1} = \boldsymbol{x}_{te} + \frac{1}{4} V_c \partial t \boldsymbol{e} \tag{8}$$

where **e** is a unit vector tangent to the blade surface at the trailing

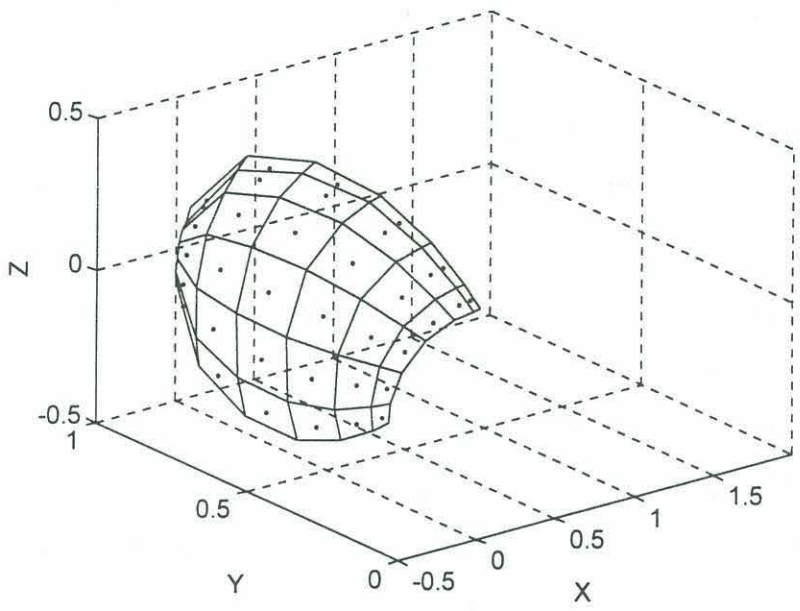

Figure 2: Discretized representation of blade for use with Vortex Lattice Method. DTNSRDC propeller 4118.

edge. The convection velocity V_c is given by

$$V_c = (\boldsymbol{v} + \boldsymbol{x}_{te} \times \Omega) \cdot \boldsymbol{e} \tag{9}$$

where $\mathbf{v}$ is the background velocity and Ω is the angular velocity of the propeller [11].

The last streamwise control points are placed on the trailing edge of the blade. Solving the boundary value problem at these locations ensures that the flow at this location is smooth and tangential to the mean camber surface of the blade, resulting in an implicit solution to the Kutta Condition. This requirement states that the flow at the trailing edge must be finite. Meeting the Kutta condition leads to the correct circulation on the blade.

Simplified versions of this procedure, including the one used in this study, place the wake on the helical path that the blade would trace through the fluid. This is referred to as rapid relaxation and

trades some of the accuracy of the solution for computational efficiency. The chord-wise elements in the wake align with the chord-wise elements on the blade. The locations of the span-wise elements in the wake, used in unsteady problems, are determined by the amount of advance of the propeller in one step of the discretization of the problem. More complex methods incorporate empirically determined concentration of vorticity at the hub and tip vortices as well as deformation of the wake due to its own induced velocities.

Solving the boundary problem (equation 7) requires determination of the flow velocities at each control point. The flow in this problem is composed of three components. The first is the speed of the propeller's advance through the water, or the ship speed. The second component is due to the rotation of the blade, or

$$\Omega r \tag{10}$$

where Ω is the angular velocity of the propeller and r is the radius of the control point being considered.

The third component is the induced velocities due to the vortices used to represent the blades and wakes. Where the first two components are given as part of the problem, the induced velocities must be solved for, and this is the bulk of the problem. The strengths of the vortices are unknown, but the influence that each vortex will have is a function of the known geometry and can be determined for a unit strength vortex.

A steady state problem is started by assuming that the wake is established and of constant strength. The vortex elements are organized in a series of "horseshoes", one for each control point. These extend from infinity to the span-wise blade element upstream of the control point, run along the blade element, then return to

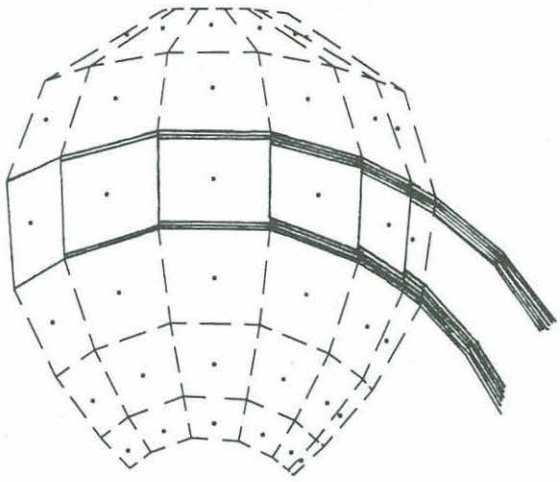

Figure 3: Illustration of horseshoe vortices on blade and wake.

infinity, as in figure 3. This arrangement satisfies Kelvin's theorem.

The boundary value problem can be written as

$$\sum A_{ji} \bullet \Gamma_j + \overline{n_i} \bullet \overline{V_i} = 0 \qquad (11)$$

where the summation is over j, for j = 1, 2, ..., (M x N), for i = 1,2,...,(MxN), M being the number of span-wise panels, and N the number of chord-wise panels. **A** is an influence matrix, composed of the influence of the ith vortex on the jth control point assuming a vortex strength of unity, and Γ is a vector composed of the unknown vortex strengths. $\mathbf{V_i}$ is the velocity at the ith control point due to inflow and propeller rotation, which are known. The boundary value

problem can be rewritten as

$$\sum A_{ij}\Gamma_j = -\overline{V_i}\bullet\overline{n_i} \tag{12}$$

with the summation the same as for equation (11). This results in a series of M x N equations and M x N unknowns, and permits the straight forward solution of the problem through the use of standard linear algebra techniques.

The solution of this problem requires determination of the induced velocity of each vortex element on each of the control points. This is accomplished with the application of the law of Biot-Savart. The induced velocity at a field point, $\mathbf{v}_{fp}$, is

$$\boldsymbol{v}_{fp} = \frac{\Gamma}{4\pi}\int_c \frac{d\boldsymbol{\xi}\times\boldsymbol{R}}{\boldsymbol{R}^3} \tag{13}$$

where **R** is the vector from each point along the curve of integration to the field point. When Γ is set to unity, this results in a vector component of the influence matrix **A** of equations (11) and (12.) While solving this equation for a helical wake would be horrendous, the discretization of the wake into a series of straight line elements simplifies the solution to merely tedious. As outlined in Kerwin and Lee [9], the solution for one straight vortex element becomes

$$\boldsymbol{v}_{fp} = \frac{\Gamma}{4\pi d}\left(\frac{e}{c} + \frac{a-e}{b}\right) \tag{14}$$

where

$$a=\sqrt{(x_2-x_1)^2+(y_2-y_1)^2+(z_2-z_1)^2}$$

$$b=\sqrt{(x_2-x)^2+(y_2-y)^2+(z_2-z)^2}$$

$$c=\sqrt{(x_1-x)^2+(y_1-y)^2+(z_1-z)^2}$$

$$d=\sqrt{c^2-e^2}$$

$$e=\frac{a^2+c^2-b^2}{2a}$$

In this case, (x,y,z) is the coordinate of the control point; (x_1,y_1,z_1) and (x_2, y_2, z_2) are the endpoints of the vortex element.

3.3 Numerical Simulation in Unsteady Flows

The vortex lattice method was used by Keenan to study propellers subjected to unsteady flow [10]. Unsteady in this context refers to nonuniform inflow velocities. Under these conditions, a propeller making one revolution encounters variation in flow velocity depending on angle of rotation. These flows are still steady in the sense that the propeller encounters the same variations at the same angle on each revolution. This condition arises frequently in the operation of a marine propeller, and can be caused by such things as wake deficits due to the ship hull upstream of the propeller or the presence of stators upstream.

The significant difference between the steady problem and the unsteady problem is the span-wise vorticity in the wake. The variation in inflow velocity creates a change in the circulation on

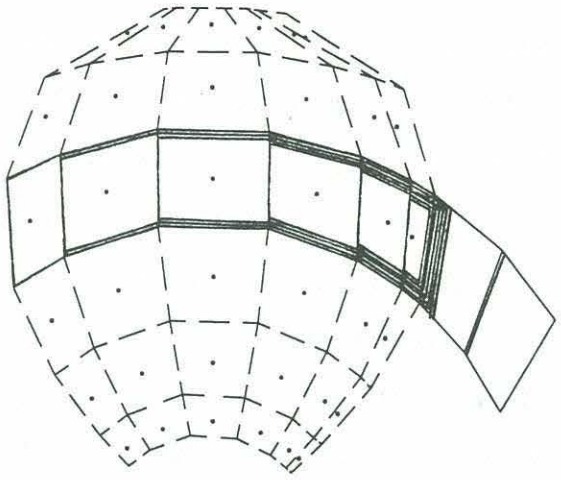

Figure 4: Illustration of wake for unsteady proble, with the vortices arranged as loops.

the blade. This in turn results in the shedding of span-wise vorticity into the wake of equal but opposite strength to the change on the blade. To represent this in the computer code, the wake vorticity is arranged as a series of loops rather than as horseshoes, as shown in figure 4. Each loop is of constant strength to satisfy Kelvin's theorem. When this loop structure is used in a steady problem, the cross element of one loop will be of equal strength but opposite sign as the cross element of the adjoining loop that is occupying the same space. These two will cancel the influence of each other, and the end result is that the loop wake reduces to the horseshoe wake of the steady problem. In the unsteady problem, the cross elements are unequal by the amount of change in circulation on the blade and do not cancel each other. The remainder is equivalent to the unsteady vortex shed into the wake by the propeller.

The problem is started by running a steady state operating

condition, which establishes the wake geometry and an initial set of vorticity strengths. The horseshoe vorticity elements are then rearranged into vortex rectangles. The variations of the problem are then introduced in a step by step fashion. Each step is a fraction of a revolution, typically one thirtieth. Keenan [10] found that convergence was typically achieved in two revolutions.

The structure of the boundary value equation is rearranged slightly due to the known value of the circulation in the wake. The unknown vorticity is now limited to the blade circulation and the first vortex in the wake. The rest of the vorticity in the wake is known and included in the right hand side of equation (12). The problem is solved for the inflow conditions at the location of the blade.

For the next step, the wake is convected downstream in the ship-fixed reference frame. The propeller is advanced one step and the sum of the circulation on the blade is shed into the wake at the trailing edge. The difference between the shed circulation of this step and the previous step is equal to the change in circulation on the blade, and results in the unsteady shed vortex. This is repeated until the problem converges.

Chapter IV Simulation of Transient Operations

4.1 Starting Point

Development of a numerical simulation for this project was based on an unsteady vortex lattice propeller code called PUF5, developed at MIT. The version of PUF5 used was part of the SPINDLE series developed by Keenan to permit studies of the affects of rotating the blades to allow the pitch to vary depending on position. This technique allows the propeller to be optimized to account for the presence of wake deficits. This feature was not used for this project.

The code was simplified in the treatment of wake roll-up. Original propulsor studies, and this project, treat the wake of the propeller as following the trace of the trailing edge of the blade through the water. This is known as "rapid relaxation" and assumes that the wake retains this helical shape forever and extends back to the starting point without deformation. This treatment was used for simplicity and computing efficiency, at the price of reduced accuracy. Figure 5 shows a blade and its wake, as discretized for the code used in this project. The original SPINDL code allows for deformation of the wake as it is convected downstream. This deformation includes roll-up of the tip vortices, where a substantial portion of the vorticity is located, as well as deformation due to the induced velocity of the wake on itself.

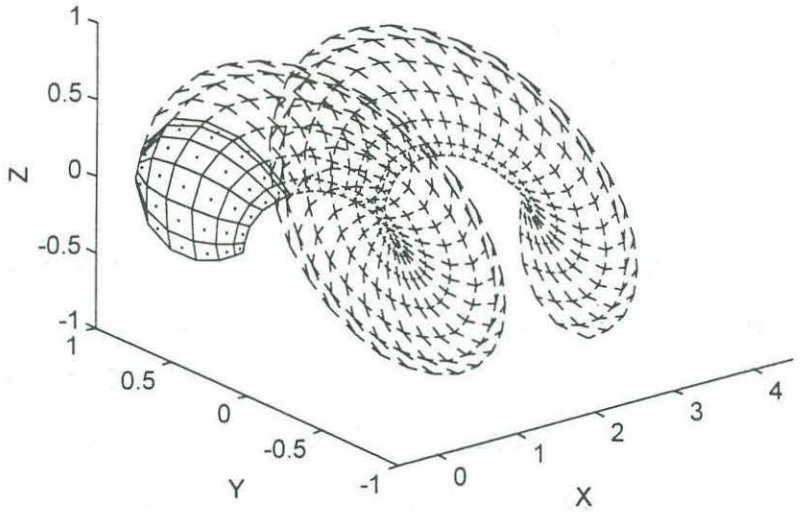

Figure 5: DTNSRDC 4118 propeller blade and wake in transient operation.

4.2 Operation of the Code

The code places the propeller in a ship fixed reference frame, aligning the positive X axis with the direction of positive inflow into the propeller. A right hand coordinate system then places positive Y to starboard and positive Z upwards. (figure 5)

The basic operating procedure of PUF5 was retained. The problem is started by solving for a steady state solution. This assumes a constant inflow velocity for a given radius, though allowing for variations in axial, radial and tangential flow components with radius. This steady solution establishes the wake vortex geometry and strengths.

The code is then operated in transient mode, iterating the rotation of the propeller and varying the strength of the vortex elements shed into the wake depending on the new operating conditions that the propeller encounters as a function of spatially varying

conditions. It is in this latter mode that the new code differs from PUF5 and SPINDL. The new operating conditions that are encountered are now variations in either ship speed, propeller angular velocity, or both.

The revolution of the propeller is discretized into a user determined number of steps. The amount of time per step is then a function of propeller angular velocity. The inflow conditions for each step are determined from three conditions. The first two are ship speed and propeller angular velocity, both of which are obtained from a user supplied file. The third is from the induced velocity created by the existence of the wake and the other blades. This inflow condition determines the vorticity strength on the blade through solution of the boundary value problem of equation (7).

When the propeller is advanced one step, the vorticity in the wake is convected downstream relative to the propeller. The rotation of the propeller results in the shedding of a vortex element into the wake. The value of this shed vortex is the sum of the chord vortex elements at each span. The loop structure of the wake places this vorticity coincident with the vorticity of the previous wake, but in the opposite direction. The result is the difference between this shed vortex and the shed vortex of the previous step and is equal to the change in circulation on the blade. The next ship velocity and angular velocity are then read in from a user supplied file and the solution to the boundary value problem is computed again for the new wake configuration.

4.3 Adaptations

Adapting the code required only minor changes to the routines

developed by Keenan [10]. The most significant change involved determining the location of the trailing edge vortex of the blade, which is also the location of the first segment in the wake. The placement of this vortex is important because the last control point must be placed on the trailing edge of the propeller in order to implicitly meet the Kutta Joukowski condition of finite velocities as previously discussed. The location is a function of ship speed and propeller angular velocity, as described in section 3.2. These were held constant in the previous program. In the new code, changes in these elements require adjustment to the vortex position at each step in the unsteady solution.

Care had to be taken in the treatment of the end of the wake in the transfer from the steady initial solution to the transient problem. The two portions of the code are different in that the solution of the initial condition treats the wake as a horseshoe while the transient condition treats it as a collection of closed loops. This should result in the same answer in a steady condition, because in this case the cross elements will be of equal strength but opposite signs and will cancel. There was a difference however. Where the horseshoe is open at the 'end' of the wake, the steady unsteady solution is closed at the end. This is because, while the previous cross-elements cancelled each other out, there is no final cross element to cancel the last, leaving it and the resulting induced velocity in place. This extra element is well downstream and the resulting induced velocity is insignificant in the overall scheme. It did create a troublesome inconsistency between the two portions of the code. The solution was to set the strength of the final element equal to zero before computing induced velocities.

Other differences are bookkeeping. The user must provide an input file containing the ship speed and propeller angular velocity at each step in the transient problem. These are read in, non-dimensionalized and stored for use in the program.

4.4 Determination of Wake Length

An important consideration in the numerical model is the length of the wake retained. In idealized theory, the wake is continuous from the propeller to the starting vortex infinitely far downstream. Retaining the wake for this length is clearly frivolous, since a vortex far away will not have any affect on a real world propeller. Furthermore, the demands on the computer system to store such a wake, much less compute the influence of the wake elements on the blades would be exorbitant. However, if the retained wake is too short, it will affect the accuracy of the solution.

To determine an acceptable length of retained wake, the circulation on a three blade propeller was computed at a radius of approximately $r/R = 0.7$ for several different wake lengths. The problem presented was the impulsive start problem, in which it is assumed that the propeller goes from a steady position of 0 ship speed and $\omega = 0$, to some nonzero ship speed and ω instantaneously. The problem was run several times with various lengths of wake retained. The results are shown in figure 6.

There are two things to note in this figure. One is that the steady state results vary widely with wake length until a wake length of about two propeller diameters, where the results converge. This is consistent with other tests run with this code and with the results obtained by Keenan. [10]

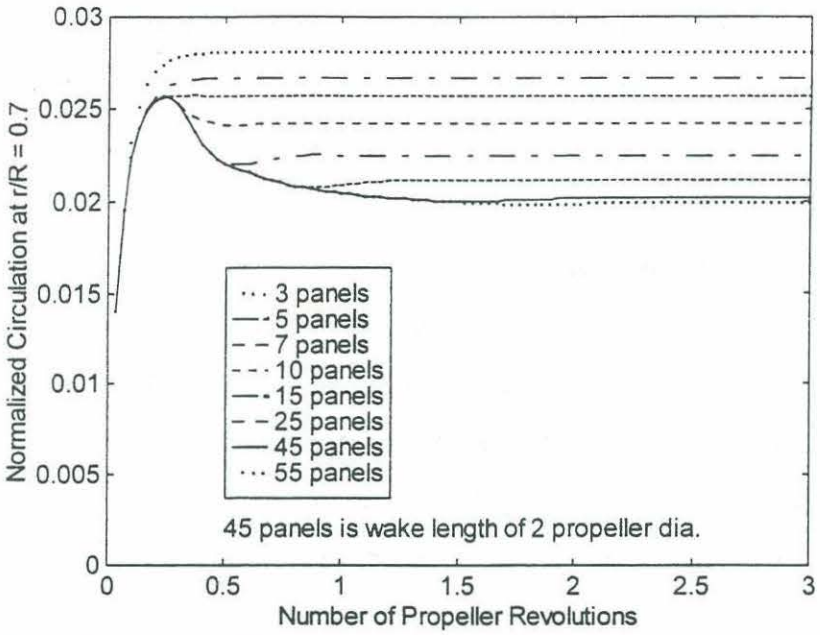

Figure 6: Effect of wake length retained on strength of circulation on blade. Simulation run using 3 blade Vetus propeller.

The second is the behavior of the wake. For extremely short wakes (less than seven streamwise elements retained), the circulation on the blade rose quickly, then approached a final steady state value from below. This behavior is similar to the start-up behavior expected in a two dimensional foil problem. In that case, the lift force achieves an initial value of one half of the steady-state value. Ninety percent of the steady lift is achieved in about six chord lengths. [12]

The behavior changed however as more and more of the wake was retained. The circulation shape developed into an overshoot, and approached a final value asymptotically from above. This overshoot behavior can be explained by considering the path of the starting vortex. This first vortex to be shed is extremely strong. Initially, it suppresses the circulation on the blade. As it is convected further and further downstream it has less of an effect on the blade,

and therefore the circulation increases. Unlike a simple foil, the helical wake of the propeller keeps the starting vortex in the vicinity, and the starting vortex of one blade very quickly interacts with the following blade at extremely close range. In the case of figure 6, at seven steps down stream the starting vortices are in a position to affect the following blade and drive down its circulation.

4.5 Steady State Results

Validity of the numerical model comes in part from being able to run the transient mode with a steady input and obtain steady results. This was done for a variety of conditions and proved to be stable. Figure 7 shows the results of one such run.

There are some very slight variations in the results, on the order of 0.01%. This minor discrepancy is due to very small deviations in the end points of the propeller and wake lattice segments which arise from the geometric constructs of the code. The blade and wake are rotated by taking the current positions of the nodes and rotating them the fraction of the revolution specified by the user. If there were no round-off errors, one could rotate one of the elements 1/30th of a revolution thirty times and the element would wind up in the exact same spot. Computers are notorious for round off errors, however, and particularly in the use of trigonometric functions.

The error has been minimized through the use of double precision. It could be minimized further through a change in the advancing algorithm. The program could retain the original position of the propeller and compute the new position relative to the original position instead of relative to the previous position. In this

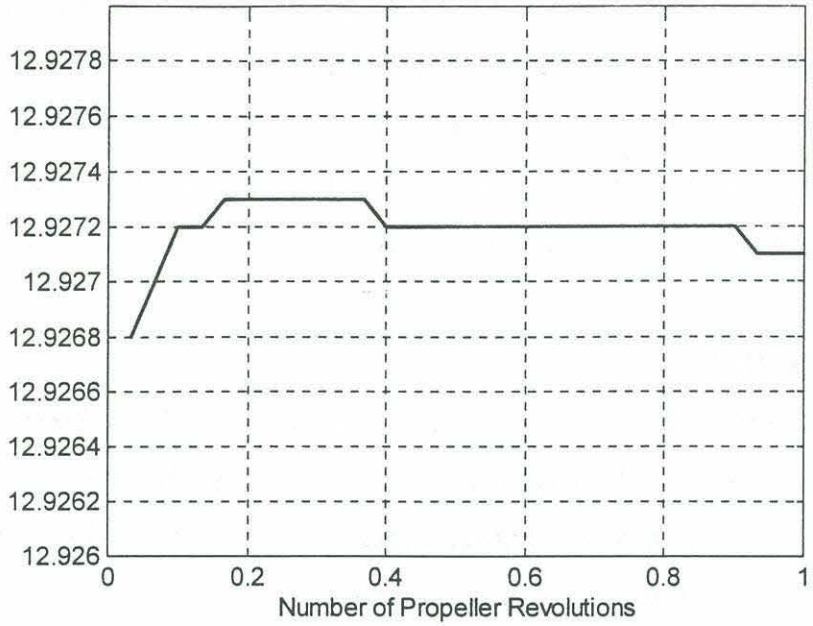

Figure 7: Three blade Vetus propeller simulation at J = 0.8. Steady state run made using transient portion of code.

method, instead of advancing one segment each time from the previous position, the advance would be one segment from the initial position the first time, two segments from the original position the second time, and so on. This would result in a small but noticeable improvement in the accuracy of the code.

There is a problem in the code which is much more serious. It has been traced to the original code, and was not introduced by the changes for studying transient behavior. Figure 8 is a plot of thrust and torque coefficients versus advance coefficient. This is a classic representation of propeller performance which unfortunately does not follow the classic shape. The curves shown should continually decrease, such as figure 1. At low J values, the curves are actually increasing, which is not physically correct. This problem probably went unnoticed originally because most propellers operate with advance coefficients greater than 0.6. In that area, the code is correct.

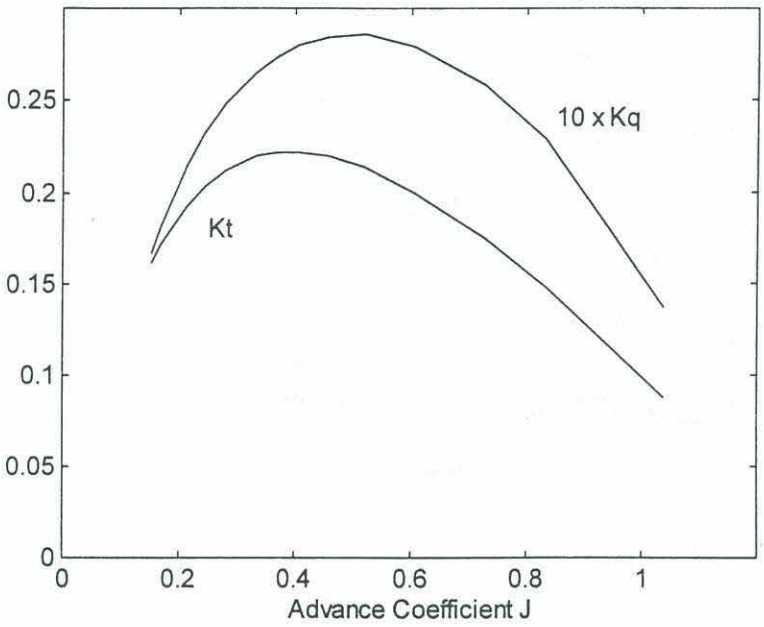

Figure 8: K_t and K_q curves generated by numerical simulation for Vetus propeller.

The transient version of the code will be used for propellers operating in the full range of advance coefficients, making this error critical.

4.6 Transient Results

It was originally hoped that numerical simulations of transient propeller operations could be made to match the situations observed in the experiments presented later in this paper. The error in the coding made this impossible, since the thruster used in the experiments operates in the range of advance coefficients less than 0.3, where the code is extremely incorrect. Transient runs were made in the region of advance coefficients for which the code shows at least the correct general behavior. These runs can be compared to the experimental results for confirmation of the general trends. Specific magnitudes are incorrect.

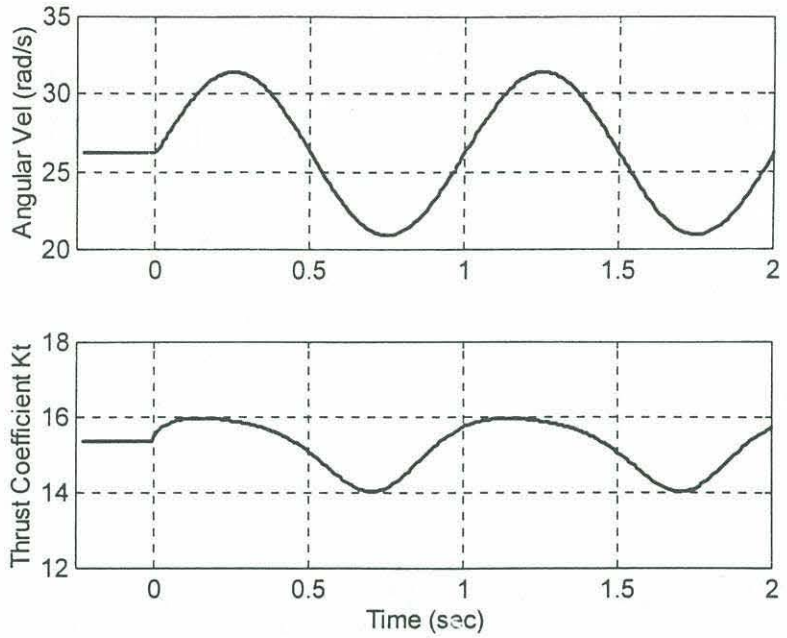

Figure 9: Numerical simulation of Vetus propeller undergoing sinusoidal change in angular velocity.

Figure 9 was run using a sinusoidal perturbation on top of a base run of J = 0.8, based on a ship velocity of 0.822 m/s and propeller angular velocity of 26 rad/s (250 rpm). The amplitude of the perturbation was 5.24 rad/s (50 rpm). The period was one second. The propeller used for the simulation was the three bladed Vetus propeller used in the experiments discussed in chapter 5.

In this run, the thrust appears to lead the velocity. In the initial increase, the thrust develops very rapidly and actually begins to decrease before the time of maximum velocity. The drop off with decreasing velocity is initially shallow, but then changes rapidly and bottoms out before the velocity. The thrust leads velocity again during the second period, with a smoother transition than the initial increase.

An explanation for this behavior in the numerical model can be

found in figure 6. This plot of the impulsive start results for the Jason propeller gives some indication of the affect of the starting vortex on the lift developed by the following blades. In the case of rapid acceleration of the blades, a powerful vortex is shed that momentarily increases the lift developed by the following blade by creating induced velocities that increase the apparent angle of attack. After the blade passes the shed vortex, the induced velocity serves to decrease the angle of attack, suppressing the lift. This provides the overshoot shown in the figure and can explain the behavior seen in the transient simulation.

The deceleration of the propeller results in the reverse behavior. In that case, the shed vorticity initially suppresses the decrease in circulation on the following blade by inducing velocities which increase the apparent angle of attack. Later, the interaction of the shed vorticity decreases the apparent angle of attack, enhancing the decrease in circulation and providing an undershoot. The combination of this acceleration and deceleration behavior results in what appears to be the change in thrust leading the change in velocity.

Chapter V Experimental Analysis of Transient Operation

5.1 The MIT Water Tunnel

The experiments were conducted in the Water Tunnel at the Massachusetts Institute of Technology. This permitted the propeller to be tested under a variety of conditions and permitted the opportunity to investigate the use of Laser Doppler Velocimetry in obtaining velocity data.

The Water Tunnel was built in 1938 as a test bed for propellers. It consists of a rectangular two story tall tunnel. Curved sections and turning vanes at the elbows facilitate even flow at the corners. The test section is located at the top of the tunnel. It is 50 cm high, 50 cm across, and roughly one meter long. A 5:1 contraction section just upstream of the test section promotes uniform flow. Two inch thick removable Plexiglas panels at the test section facilitate installation and observation of the experiments.

An impeller is located at the opposite side of the tunnel. It is capable of driving the flow in the tunnel at up to 9 meters per second and is used to simulate the desired ship speed. It is limited in that it is intended to create flows exceeding one meter per second, is difficult to control below 0.5 meters per second, and does not operate at less than 0.25 meters per second. This experiment was concerned with operations of vehicles that are typically operated at velocities below 0.5 meters per second.

A differential pressure cell in the contraction section is used to measure nominal flow velocity. A vacuum pump is available to permit variation of the pressure in the tunnel for use in cavitation experiments. This was not used in this experiment.

The facility is also equipped with a Laser Doppler Velocimetry system. This system uses the doppler shift in the light reflected from a seed particle passing through the interference pattern of a pair of intersecting laser beams to determine the point velocity in a flow. The advantage to it is that it is a non-intrusive system. The only effect on the flow is the effect of seeding the flow with extremely small (< 10 micron diameter) neutrally buoyant particles.

There are three disadvantages to the LDV system as far as these experiments were concerned. The first is that it only provides a point measurement. Steady-state flow experiments can construct the full velocity field from a collection of point measurements taken one at a time. For transient experiments, this would require repeating the transient conditions many times.

The second is that there are some variations in the data, and to be used effectively the data needs to be averaged over 150 points. The transient conditions being considered in this series of experiments happened very quickly. In the case of step changes in particular, the LDV velocity data arrived too slow to permit averaging of five or ten points, much less 150.

The third is that velocity data can only be obtained at the time that a particle passes through the interference pattern and can not be timed to occur at the time of the transient events. This is particularly problematic in low flow velocity experiments where the time between particles can approach one second or more. The dynamics

associated with rapid changes in propeller velocity can be over within one second, and the associated changes in local flow velocity would be completely missed if it occurred between particles.

5.2 Thruster Mount

The water tunnel is equipped with a propeller shaft that is normally used for propeller tests. It is designed for use with steady state tests and the inertia of the shaft as well as the control system available made using this shaft impractical for these experiments. (It was used for the earlier steady state experiment that generated the data presented in figure 1).

To get around this limitation, a thruster from the ROV *Jason* was mounted in the tunnel test section and used to operate the propeller. The thruster was suspended from the rudder dynamometer, which was designed for testing forces and moments on rudders and other lifting surfaces in steady operating conditions. It was installed in place of the top window of the test section. A series of six load cells were installed to provide data on the forces and moments applied to the support shaft.

For the experiment, a mount was made from aluminum which held the body of the thruster motor at the center line of the tunnel. The thruster is normally mounted to the vehicle at the shroud, but this was not appropriate since tests were conducted with and without the shroud in place. The aluminum mount was welded to an 1.5 inch aluminum shaft which proceeded up and into the rudder dynamometer.

5.3 Thruster Specifics: Motor and Propeller

The thruster motor was a Moog DC brushless servo-motor, model

304-140A, in a custom oil-compensated housing. A resolver provided feedback to a resolution of 4096 points per shaft revolution. Manufacturer data provided a calibration of 0.7874 amps per Newton-meter.

The motor used was oil compensated. In this design, the motor and the accompanying 1" diameter hose carrying the necessary wiring is filled with a nonconductive mineral oil. The assembly is connected to a pressure compensator by a second hose, 5/8 inches in dia. The compensator maintains the oil pressure at 1.5 psi above the ambient pressure, ensuring that the motor seals only have to resist a minimum pressure differential and that in case of a leak this differential is positive out of the motor. By mounting the compensator to the vehicle, this system allows the pressure differential to be held constant, whether the vehicle is on the surface or at 4000 m depth. For this experiment, the oil compensator was mounted outside of the tunnel. The hoses were fed through the holes in the back window of the tunnel test section.

The amplifier used was an Elmo EBAF-15/160 Servo Amplifier, designed for use with brushless DC motors. It is a pulse width modulated, full wave, three phase servo current amplifier. The switching frequency is 20 kHz. It is operated with a 120 V PS/S series unregulated DC power supply.

The amplifier was calibrated by blocking the propeller with a 2x4 and commanding a range of voltages while monitoring the amperage in the motor leads. The results of this calibration are plotted in figure 10. It shows a very linear arrangement over a wide range of both positive and negative command voltages and provides a conversion factor of 0.712 amps per Volt.

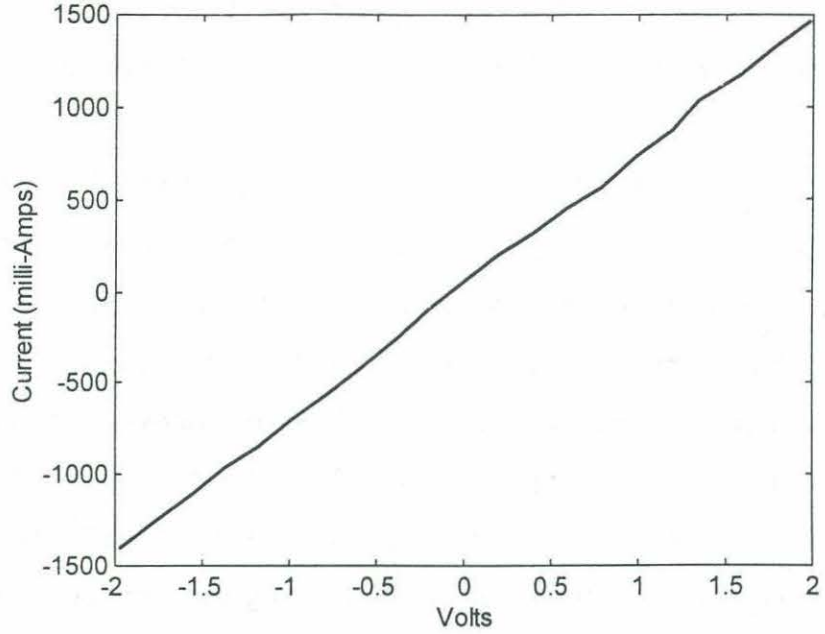

Figure 10: Calibration of Elmo servo amplifier: 0.712 Amps per Volt.

The propeller used was a 246 mm diameter three blade propeller, manufactured for the Vetus Corporation for use in their small boat bow thrusters. The hub diameter is 40 mm. The blades are symmetrical in forward and reverse, and have a pitch of 22.5 degrees. The propeller was mounted directly to the motor shaft; no gear box was used.

Tests were run with and without a duct. When a duct was used it was 260 mm inside diameter, 127 mm long. The duct was mounted to the motor housing and supported by four stators upstream of the propeller, each approximately 4 mm long tapering to 2 mm.

5.4 Experiment Operation

The experiment was controlled and monitored by a Pentium PC, 133 MHz clock speed. A program was written which controlled the motor velocity, sending commands at 500 Hz and logging data at 100 Hz. Data were stored electronically until the end of the run so that data

collection did not interfere with the timing of the motor control. The program allowed the motor to be run at a steady state velocity for an unlimited period of time prior to beginning the logged portion of the experiment in order to provide a steady state initial condition. One second after logging began, the angular velocity of the motor shaft would be varied according to a predetermined experimental plan. At the end of eight seconds the computer would shut the thruster motor down and stop logging data.

The parameters logged included a time stamp, volts commanded, actual shaft position and velocity from an internal encoder, a differential pressure cell in the tunnel wall, and the voltage output from the six strain gauges mounted to the rudder dynamometer. In addition, several diagnostic signals from the motor and the program were also logged. The experiment was primarily concerned with four parameters. The angular velocity of the propeller was obtained from the shaft encoder of the motor. The thrust was obtained from one of the load cells. Torque was obtained from the volts commanded multiplied by the volts to amps conversion of the Elmo Amplifier and by the amps to Newton meter conversion of the Moog motor. These three are considered versus time in the rest of this report.

Flow velocity data came from three sources. One was a differential pressure cell located on the tunnel wall upstream of the test section and recorded by the logging program. The second was from the impeller rpm that was generating the flow. Both are calibrated regularly by tunnel personnel. The third source was the LDV. This was used to measure velocity at two locations. One was one propeller diameter upstream. The second was downstream one propeller diameter. Both were at 0.7 radii from the centerline of the propeller shaft,

aligned with the x axis. This position was the farthest from any of the obstructions in the tunnel (hoses or support shaft.)

The LDV was run by a second computer. Coordination between the two control computers was done by a signal sent by the first computer, which instructed the LDV computer to begin. This was less than desirable since the LDV computer then assigned time zero to the next time that a particle appeared. This lag could not be determined from the data and no signal was available to identify when it occurred because of the nuances of the LDV control system. This could result in a substantial time lag for runs with low flow velocities.

5.5 Signal Noise

Extensive time was spent attempting to isolate sources of noise in the data records. There were three sources that proved to be persistent. The first was an 80 kHz noise introduced by the amplifier. It is a Pulse Width Modulation amplifier which switched at 20 kHz. It is used on the vehicle because of it's relatively good power conservation. The vehicle that the amplifier is used on consumes a fair amount of power running sonar, lights and video in addition to the seven thrusters. This power must be fed to the vehicle through ten kilometers of cable. Minimizing this power consumption is of primary importance.

Running this experiment in a lab does not have the same requirements however. Power is readily available, and the type of data being recorded is very susceptible to interference from such noise. The noise was on the order of 400 mV, while the desired signals from the load cells were in the range of -5V to 5 V. Not having to be concerned with power consumption would permit the use of

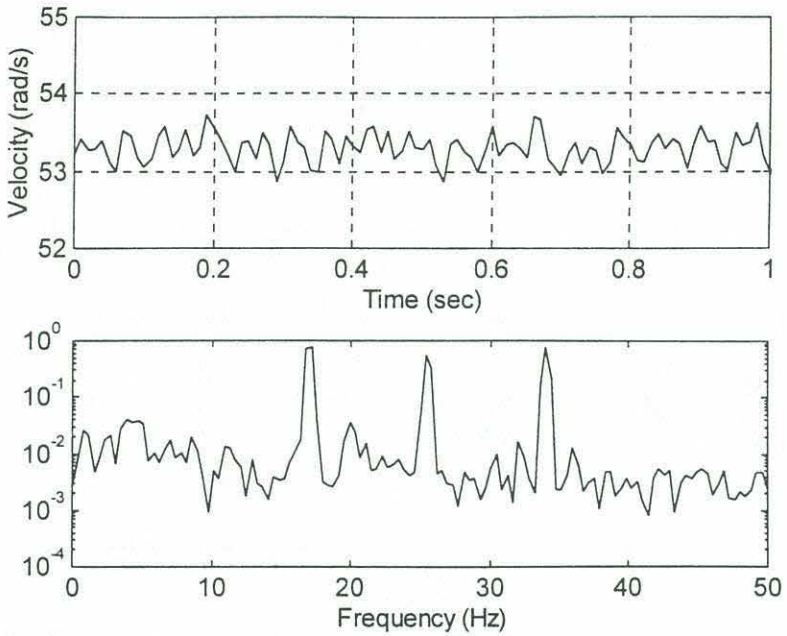

Figure 11: Steady state velocity data for run 653. Peaks in spectrum are noise from amplifier and wake deficits.

another type of amplifier which would eliminate this noise.

The amplifier was also responsible for the second source of noise, which was a variation in shaft speed of up to (+-) 0.3 rad/s at a rate of twice motor shaft speed. For example, the shaft velocity for run 653 is plotted in figure 11. It was a steady state run with a mean angular velocity of 53.3 rad/s. The velocity varied from 53 to 53.6 rad/s. The velocity spectrum is also plotted. The peaks at 16.9 Hz and 33.9 Hz are at two and four times the shaft velocity of 8.5 hz and correspond to the first and second harmonic of the variation in angular velocity caused by the amplifier. The peak at 25.5 Hz corresponds to three times the shaft velocity and is attributed to the wake deficit described in section 5.8.

The third and most serious noise source was the vibration of the rudder dynamometer. While making preliminary runs, it was discovered that propeller shaft velocities in the vicinity of 55 rad/s made the

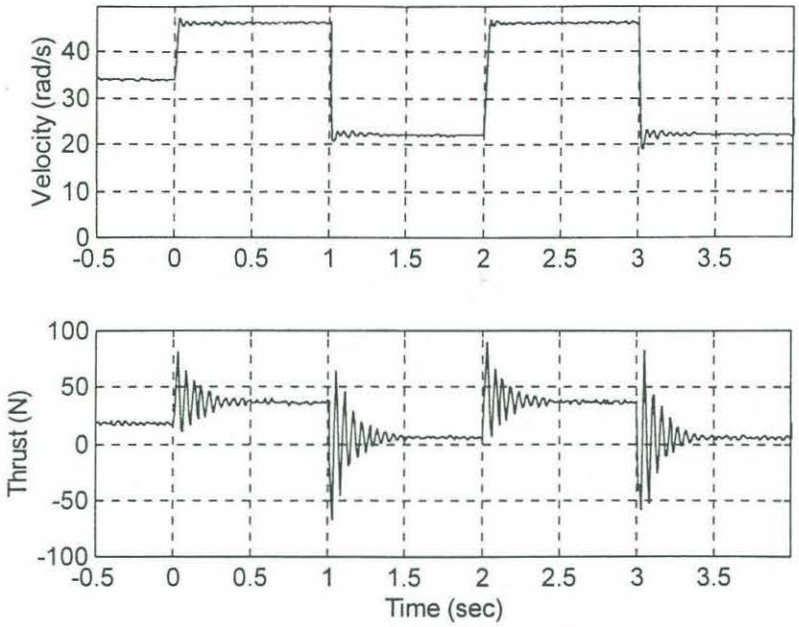

Figure 12: Velocity and thrust data from run 646. Flexibility in the dynamometer lead to excessive ringing in the thrust data.

rudder dynamometer vibrate visibly. One of the strain gauges was used as the input into an HP Spectrum Analyzer. The dynamometer was excited by a localized impact load (it was hit with a hammer.) The spectrum of the resulting vibration had a first harmonic at 18.8 Hz. It was apparent that the variation in shaft speed at 55 rad/s (8.5 Hz) resulted in varying thrust at 19 Hz which was exciting the resonant frequency of the dynamometer.

The dynamometer was designed for studying steady state loads on foils. This experiment tried to use it for varying loads. Rapid changes in thrust resulted in ringing behavior that frequently made the data unusable. This is clearly evident in figure 12. This is data from run 646 which placed a square wave perturbation of 12 rad/s (115 rpm) over a steady run of 34 rad/s (325 rpm). The excessive ringing makes quantitative analysis impossible.

5.6 Uniformity of Inflow Velocity

In an ideal experimental environment, the flow into the propeller would be uniform. The presence of the supporting stand and hoses as well as the presence of the thruster motor in the test section created variations in the flow which must be addressed. The stand and hoses created localized "wake deficits" which will be discussed in section 5.8. The body of the thruster motor created an increase in the flow, which is addressed here.

A simple analysis of the test section and an application of conservation of mass (assuming an incompressible fluid and inexpansible test section) shows that the presence of the motor in the center of the test section requires an increase in flow velocity around it. If the increase is assumed to be uniform throughout the flow, conservation laws show that a 0.095 m diameter motor body in a 0.51 m square test section will require a local flow velocity of 1.02 times the far field flow velocity.

Initially, the increase in flow will not be uniformly distributed throughout the flow cross-section. Potential flow analysis techniques can be used to obtain a first approximation of the local affect of the motor housing on the flow velocity, representing the motor as a simple sphere by using a dipole. The equation for the flow velocity tangent to the sphere at θ equal to $\pi/2$ or $3\pi/2$ (where θ equals 0 in the axial direction) is

$$V_\theta = -U\sin\theta\left(1+\frac{a^3}{2r^3}\right) \qquad (17)$$

where U is the undisturbed flow velocity, a is the diameter of the sphere and r is the distance from the center of the sphere to the point where the velocity is being considered.

The result is that the flow velocity is 1.5 U at the boundary of the body, but drops off quickly with $1/r^3$. The deviation from normal flow velocity at the tunnel wall is less than one percent. If the wall had been represented through method of images, it would have increased the flow velocity, but insignificantly when compared to the effect of ignoring viscosity.

This result can be compared with data collected using the LDV system as well as with the flow velocities obtained from the impeller speed. The LDV system was set up to record velocities at r/R = 0.7 from the centerline of the thruster, aligned with the horizontal axis of the thruster. Two laser heads were used. The primary head was located a distance of 0.5 propeller diameters upstream of the centerline of the propeller. This head had a strong signal strength and gave reasonable results. A second head, which was run through a fiber optic system, was used to measure velocities 0.5 propeller diameters downstream of the propeller center line. This head had a very weak signal and provided questionable data which was not used. Plots of the point by point measurements from both heads for run 506 are shown in figure 13.

Based on the inviscid theory, a local flow increase of 8% at the location of the laser heads would be expected. That did not occur. Tests were run with the propeller removed from the thruster and the impeller was used to generate flow through the test section. The results are plotted in figure 14. The velocities obtained with the LDV were very close to those obtained from the calibration of the Impeller. A least squares fit of the data shows that LDV velocities are 0.9912 * Impeller determined velocities for the set up with the duct. Without the duct, this increases to 1.0224 * Impeller estimated

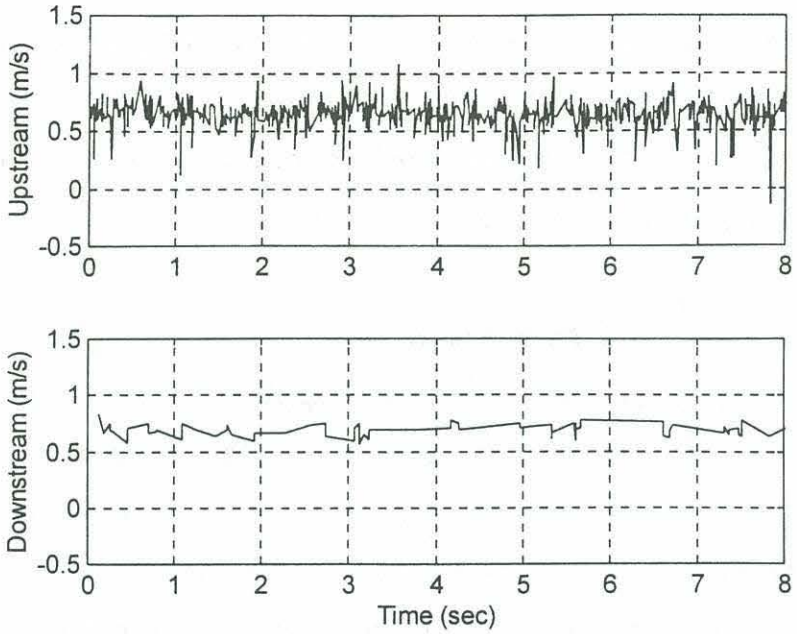

Figure 13: LDV velocity measurements for run 506 - steady state flow with propeller removed.

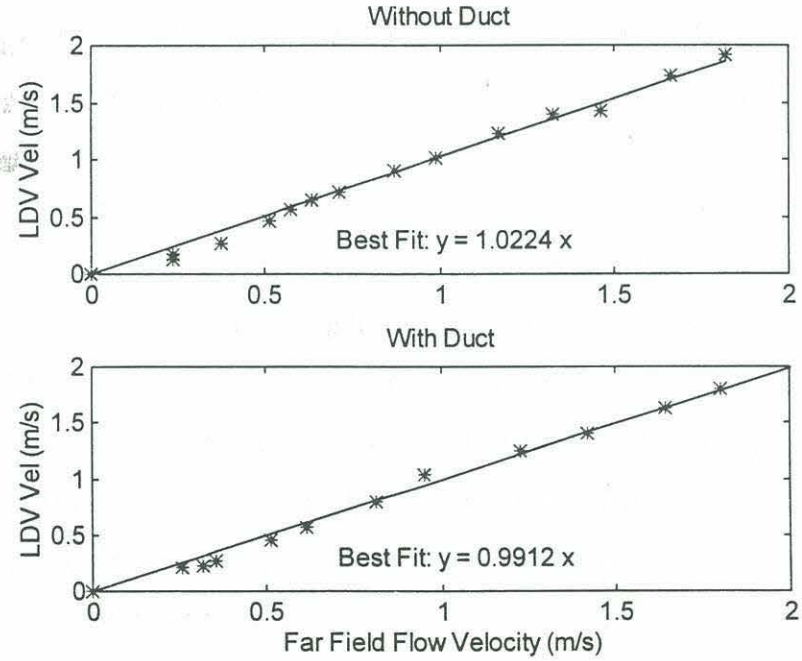

Figure 14: LDV flow velocity data versus velocity data from impeller calibration.

velocities. Discrepancies between the potential flow estimate and the LDV velocities can be attributed to momentum redistribution due to viscosity, as well as tunnel velocity defects. For example, it was noted by Lurie [12] that the tunnel has some flow discrepancies near the centerline due to allowances made for the propeller shaft, which was pulled back in this experiment.

5.7 Drag on the Motor and Test Stand

Flow past the motor and test stand applied a downstream force which was measured by the thrust load cell. The load cell was set to zero with no flow in the test section. The drag induced by the flow must be added to the thrust data to offset the affect of drag.

Tests were preformed to determine drag on the motor as a function of flow velocity. For these runs, the propeller was removed and the impeller was used to generate flow through the test section. This was done for the motor without the duct and with the duct, and the results are plotted in figure 15. The data follows a quadratic relationship as expected.

5.8 Localized Wake Deficits

Drag on objects upstream of the propeller created local decreases in flow velocity at the propeller. The sources of this deficit were the two hoses providing power and oil pressure to the motor and the aluminum shaft which supported the thruster in the tunnel. The two hoses were fairly far upstream. The support shaft, which was 1.5 inches in diameter, was close to the propeller and the primary source of wake deficit.

The decreased flow velocity entering the propeller disk altered

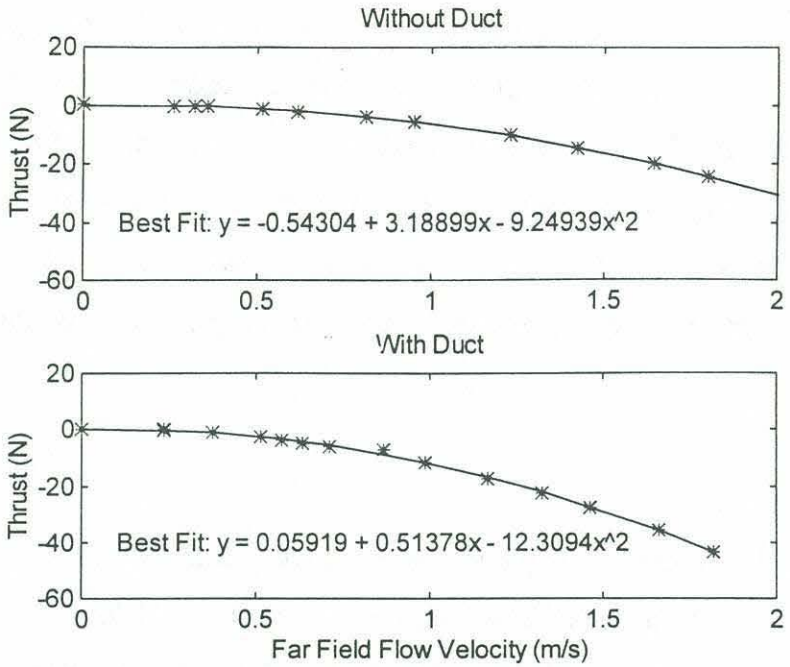

Figure 15: Drag on motor and test stand, with propeller removed. For thruster with and without duct.

the angle of attack, resulting in a temporary change in lift. In the case of the three blade propeller, there were two other blades with the typical lift applied as the key blade passed through the deficit, resulting in a temporary imbalance in the blade forces experienced by the motor shaft and ultimately by the strain gauges. This imbalance showed up in thrust measurements as a vibration with a primary harmonic at three times the shaft rate.

5.9 Experimental Results

Over three hundred experimental runs were made. Runs were made with the impeller off for a no-flow situation, as well as with the impeller set to provide an inflow of 0.24 m/s, 0.4 m/s or 0.514 m/s. The last value is the maximum velocity at which the Jason vehicle is capable of moving. The slowest velocity is the lowest velocity of flow that the impeller is able to produce. Runs were made with and

without the duct in place.

A variety of types of runs were made within the range of the above operating conditions. These included steady state operations, step changes in angular velocity, and square wave and sinusoidal perturbations on top of steady base velocities. Several different propeller speeds were used, up to about 55 rad/s (525 rpm). For the sinusoidal and square wave perturbation runs, periods ranged from 1 to 4 seconds.

5.9a Steady State

Steady state runs were made to provide data on the operating characteristics of the propeller and to assist in identifying the noise generated by the testing and data collection systems. In all cases, the thruster was allowed to run for several minutes to establish steady flow conditions before the data was logged.

Figure 16 shows the K_t and K_q curves obtained for the propeller without the duct in place. Figure 17 is the equivalent for the propeller with the duct. The K_t curves for both data sets appears reasonable, both in the magnitude and the shape of the curve.

The K_q curves suggest an error in the data. The order of magnitude is correct, but K_q should decrease with increasing advance coefficient. In most cases, increasing advance coefficients were obtained by decreasing the motor angular velocity. This may have required a disproportional amount of torque to turn the motor. Torque values were obtained from the amps drawn and the amps to Newton meters conversion factor supplied by the manufacturer. This could lead to errors in torque values if this coefficient is not constant with motor speed.

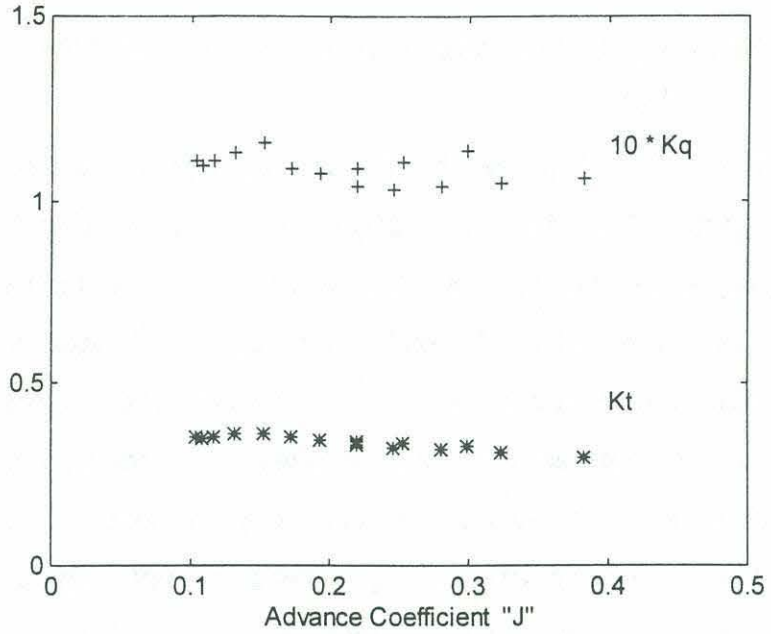

Figure 16: K_t K_q curves for thruster without duct.

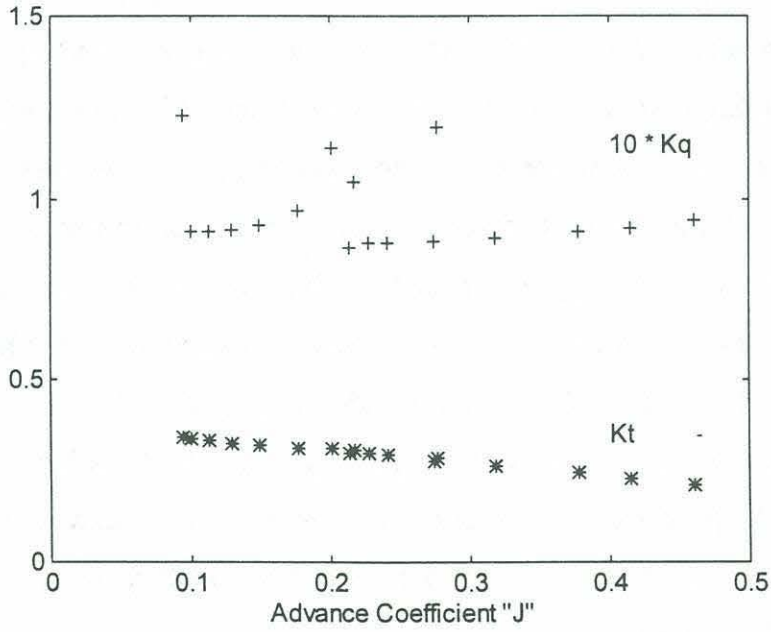

Figure 17: K_t K_q curves for thruster with duct.

In some cases, the advance coefficient was increased by increasing the flow velocity. This could contribute to the flow driving the propeller to varying degrees and could have contributed to the scatter of the values.

Figure 17 can be compared to figure 1, which is for the same propeller and duct. The data for figure 1 were obtained using the shaft in the propeller tunnel, so the effect of the thruster motor and test stand are not present. In addition, the duct was mounted in such a way that it did not contribute to the thrust measurements. The magnitudes of the K_t curves are very close. The values for torque are similar in magnitude, but do not really compare well. This can be attributed to the problems with torque measurements discussed above.

It is useful to this study to examine the steady state runs in terms of the noise that is present to corrupt the data. The velocity data from run 653 was plotted in figure 11. This was a run made without a duct, with a mean velocity of 53.3 rad/s. As discussed earlier, there are three dominant peaks in the velocity spectrum. The first, at 16.9 Hz, is at twice the shaft rate of 8.49 revolutions per second, and can be attributed to the amplifier. The second, at 25.5 Hz, is at three times shaft rate and can be attributed to the wake deficit caused by the support shaft. The third peak is at 33.9 Hz or four times the shaft rate, and is a second harmonic of the first.

The data from run 320 is plotted in figure 18. In this case, a duct was in place, and the mean velocity was 28.5 rad/s (4.5 revolutions per second). The spectral analysis shows dominant peaks at 8.9, 13.5 and 18.3 Hz, corresponding to roughly two, three and four times the shaft speed.

There are two conditions that deserve attention. One is when the

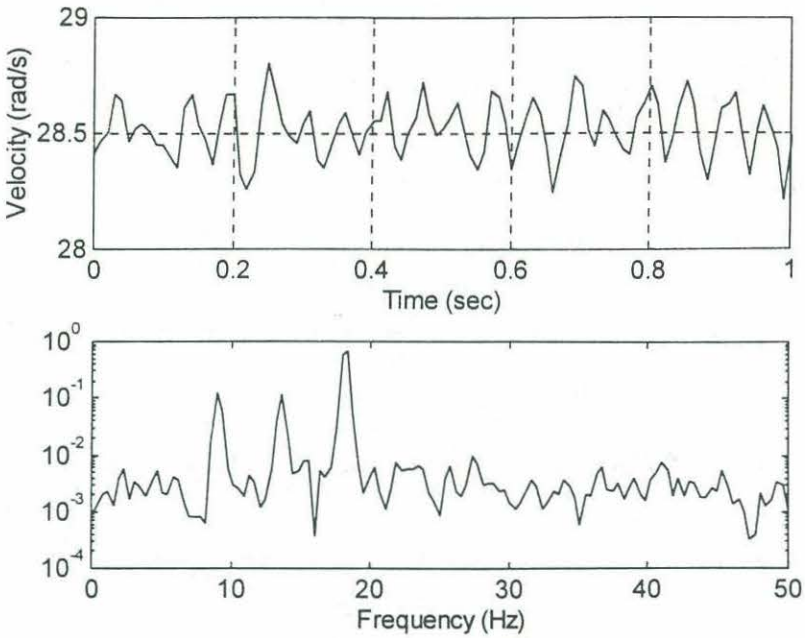

Figure 18: Velocity data from steady state run 320.

shaft speed is at roughly 9 Hz, the other a shaft speed of approximately 6.5 Hz. These cases are at one half and one third the natural frequency of the test stand, as discussed in section 5.6. The velocity data from run 323 is presented in figure 19, which was a duct run at 41 rad/s (390 rpm) mean velocity, or 6.5 revolutions per second. In this case, the wake deficit created a near resonance situation with the test stand natural frequency, causing the test stand to vibrate and disrupt the thrust load cell signal with noise. The thrust data for that run is shown in figure 20. The dominant peaks are at 13.4 and 19.5 Hz. The mean thrust was 42 N. It oscillates from 35 to 50 N.

Figures 21 and 22 are of run 657, a ductless run with a mean velocity of 59 rad/s (560 rpm), resulting in a shaft speed of roughly one half the frequency of the stand. Spectrum peaks for the velocity occur at 19, 28.5 and 38.3 Hz. The mean thrust was 24.5 N. The

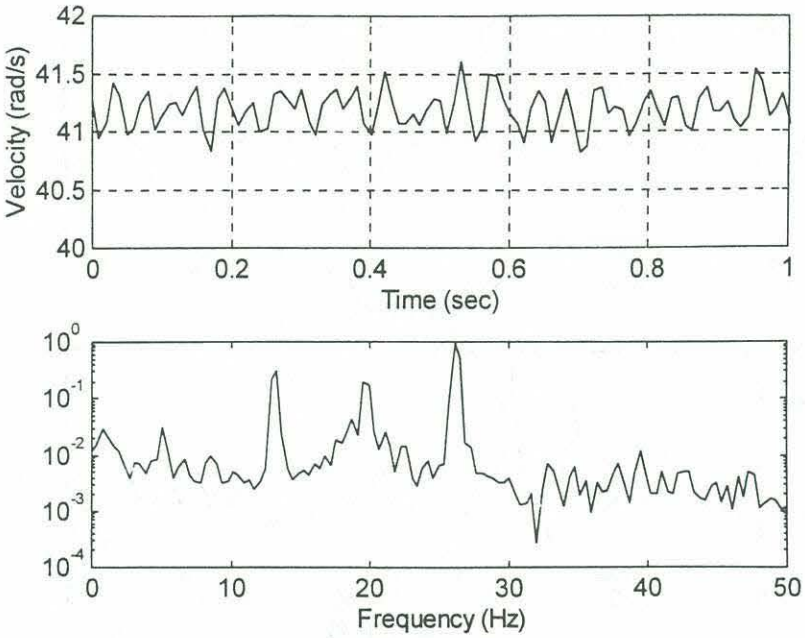

Figure 19: Velocity data from steady state run 323.

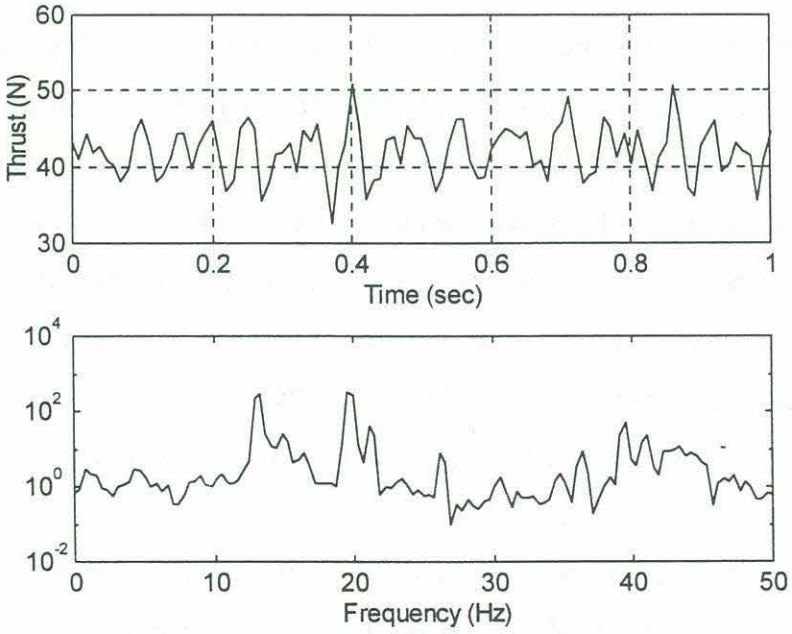

Figure 20: Thrust data for steady state run 323.

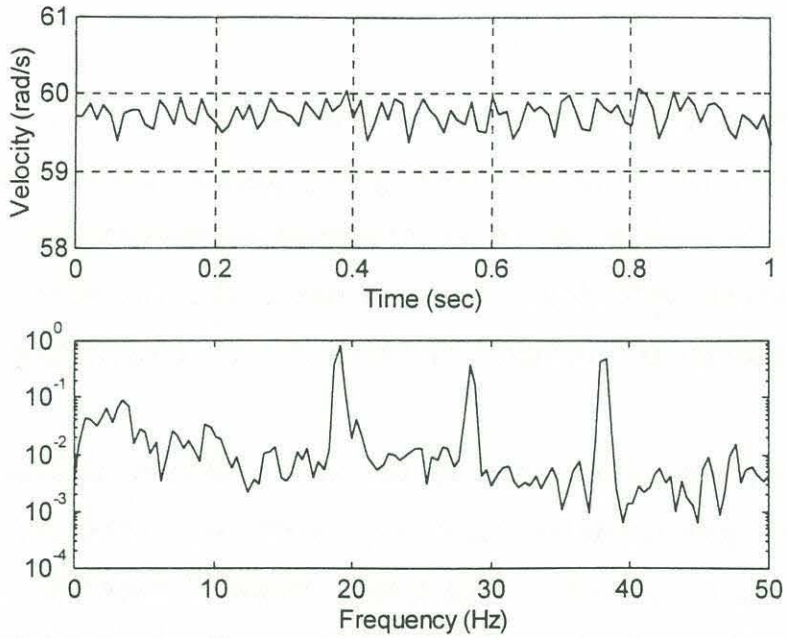

Figure 21: Velocity data for steady state run 657.

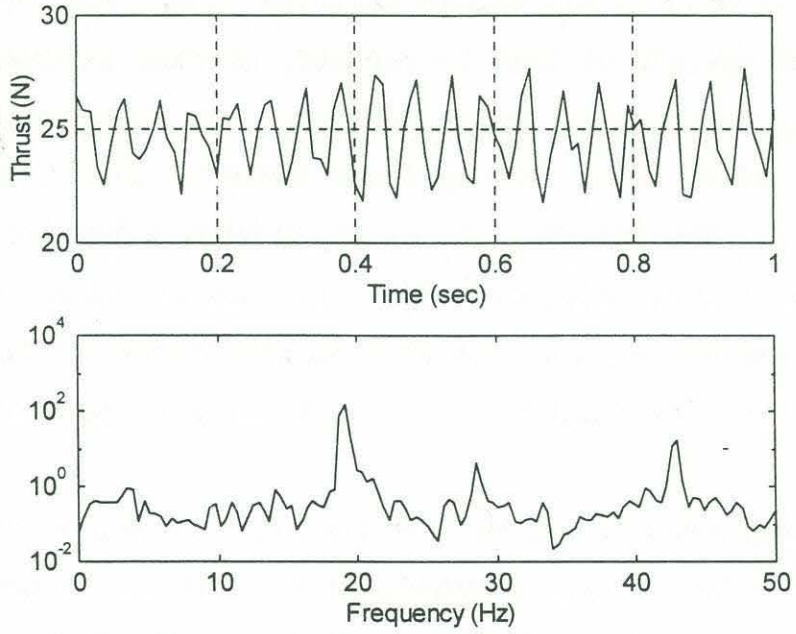

Figure 22: Thrust data for steady state run 657.

thrust spectrum is dominated by a peak at 19.16 Hz.

5.9b Step Changes and Square Wave Perturbations

The dynamics of thrusters undergoing abrupt changes in angular velocity were examined by doing experiments incorporating step changes from a steady state velocity. In each case, the thruster was operated at a steady velocity for several minutes before commanding the new velocity.

Experiments were also done in which the abrupt change was treated as a square wave perturbation on top of a steady state run, with periods from 1 to 4 seconds. These runs created significant vibrations, resulting in data which is not worth considering (see figure 12).

The abrupt changes in angular velocity created substantial overshoot and ringing in the thrust data due to the flexibility of the test stand. An example of this is run 306, plotted in figures 23 (shaft velocity and torque) and 24 (thrust). In this run, a steady state velocity of 41 rad/s (390 rpm) was followed by a jump to 54 rad/s (525 rpm). The thruster was equipped with a duct and was operating in a flow velocity of 0.514 m/s. The overshoot and ringing out in the thrust measured at the step is significant. This can be attributed to the flexibility of the dynamometer as previously discussed.

The ringing settles out in less than one second, settling down to a steady state value of approximately 84 N. The thrust continues to decrease, however. The value of the average thrust for the last second logged was 81.5, and is plotted as a horizontal line in figure

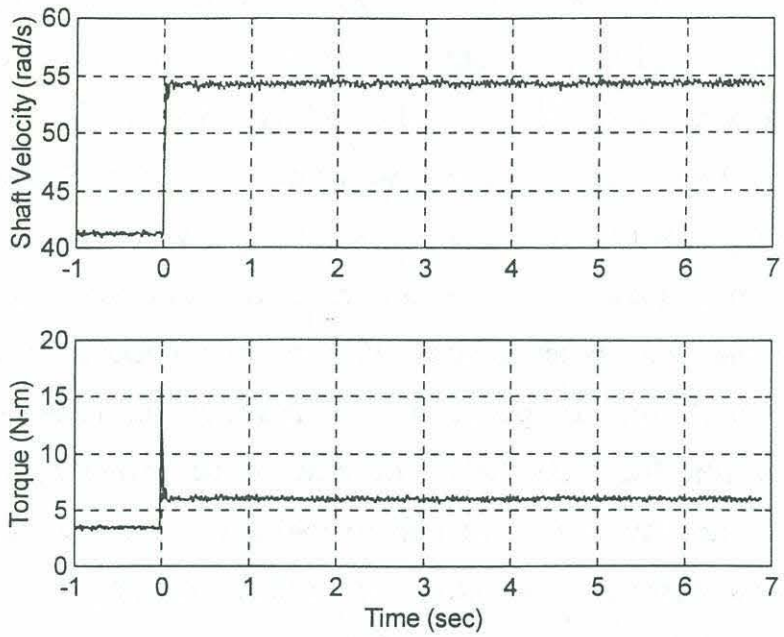

Figure 23: Velocity and torque data for run 306.

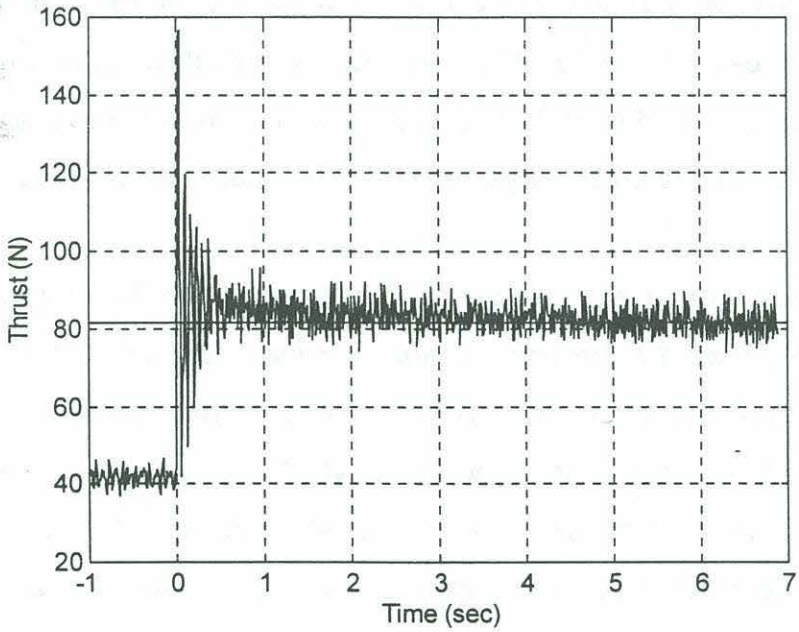

Figure 24: Thrust data, run 306. Horizontal line at 81.5 N is mean thrust of last second of run.

24. The velocity and torque reach fairly constant values of 54.3 m/s and 6.0 N-m respectively within one second of the step change.

This trend is evident in other runs and under other conditions. The velocity data from run 631 is plotted in figure 25. For this run the duct was removed. The initial mean velocity was 23 rad/s (215 rpm) and the step was to 46 rad/s (445 rpm). The thrust data for this run is plotted in figure 26. The behavior is similar to the ductless run. In this case, the mean thrust of the last second of data collection was 36 N, and is plotted as a horizontal line.

An explanation for this behavior can be obtained by considering the momentum of the fluid around the propeller. In a steady state condition, inflow velocity is constant, resulting in a constant angle of attack at the blade and constant lift. In the case of a rapid step change, the angular velocity is established well before the momentum of the inflow fluid has had time to adjust. The result is an initial increase in angle of attack relative to what the steady state velocity will eventually be. This translates into a greater lift force and resulting thrust. As the velocity of the inflow increases, angle of attack declines, and thrust approaches the quasi-steady value from above.

Run 641 was for a step decrease in angular velocity and is presented in figures 27 (velocity and torque) and 28 (thrust). This run was made with the duct in place. The initial mean velocity was 59.4 rad/s, followed by a step down to 46.7 rad/s. The change in thrust was from 25.8 N to 15.3 N, shown with a solid line. In this case, the momentum of the fluid meant a higher than normal flow after the step down, meaning a lower angle of attack than would have been experienced in a steady state condition. The consequence is an

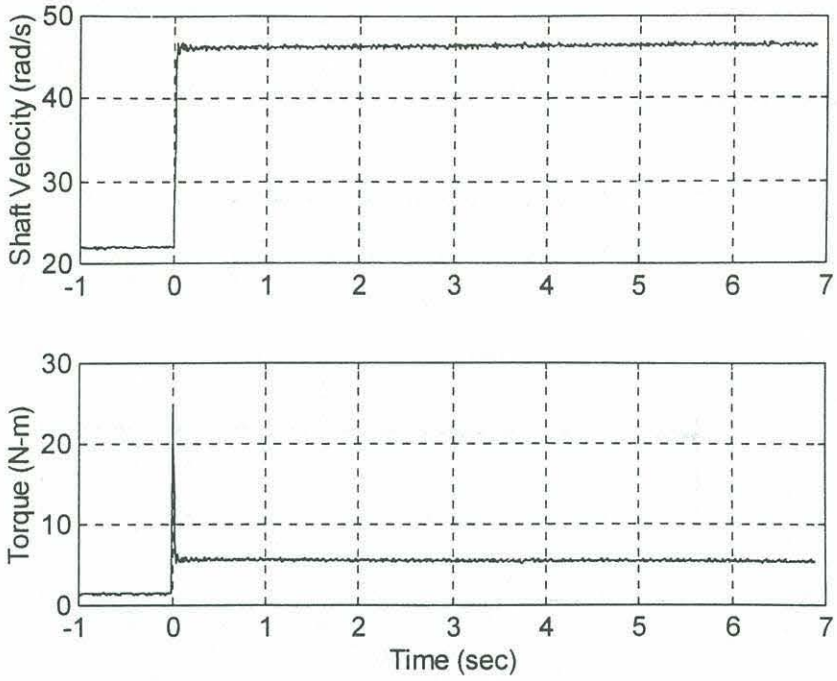

Figure 25: Velocity and torque data for run 631.

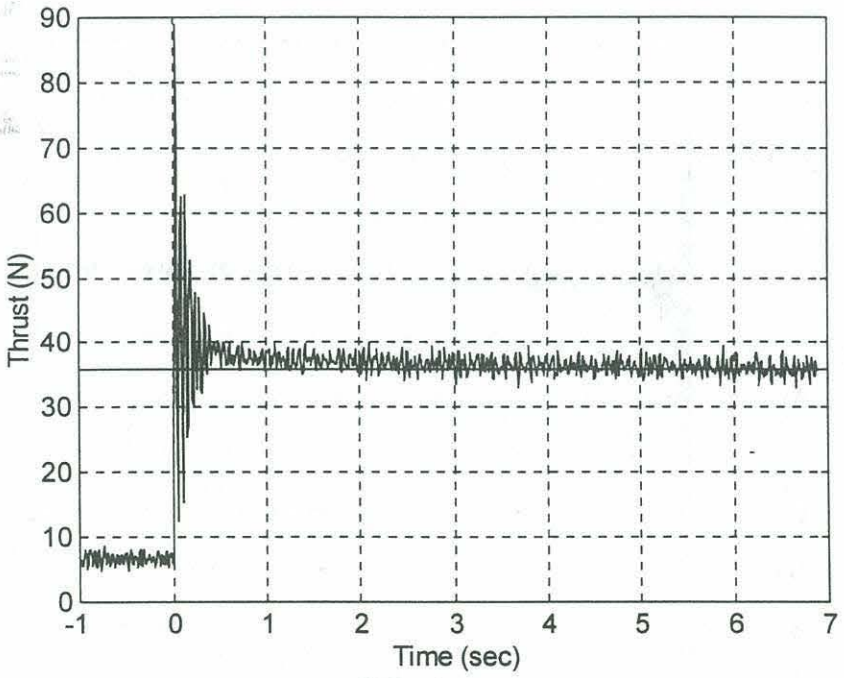

Figure 26: Thrust data, run 631. Horizontal line at 36 N is mean thrust for last second of run.

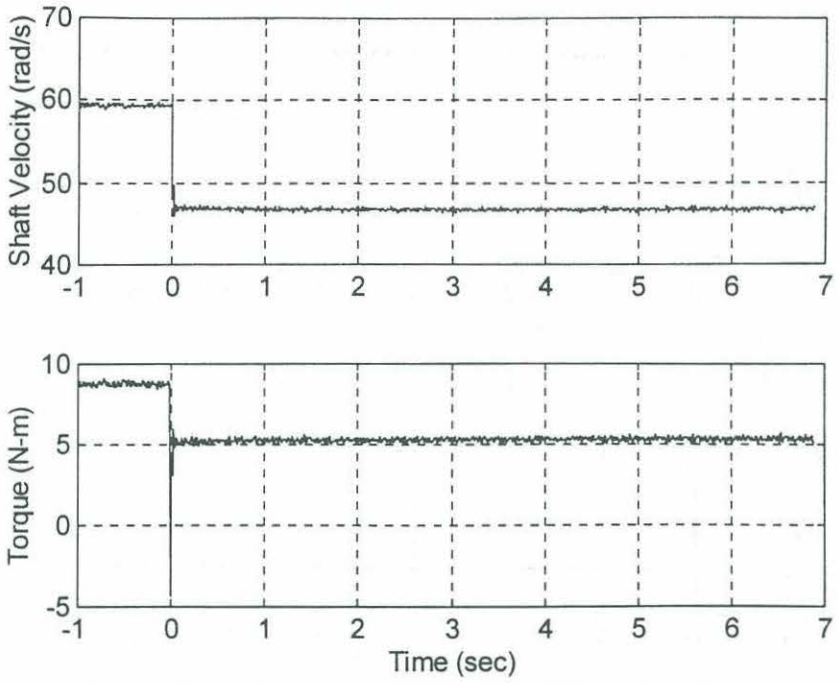

Figure 27: Velocity and torque data for run 641.

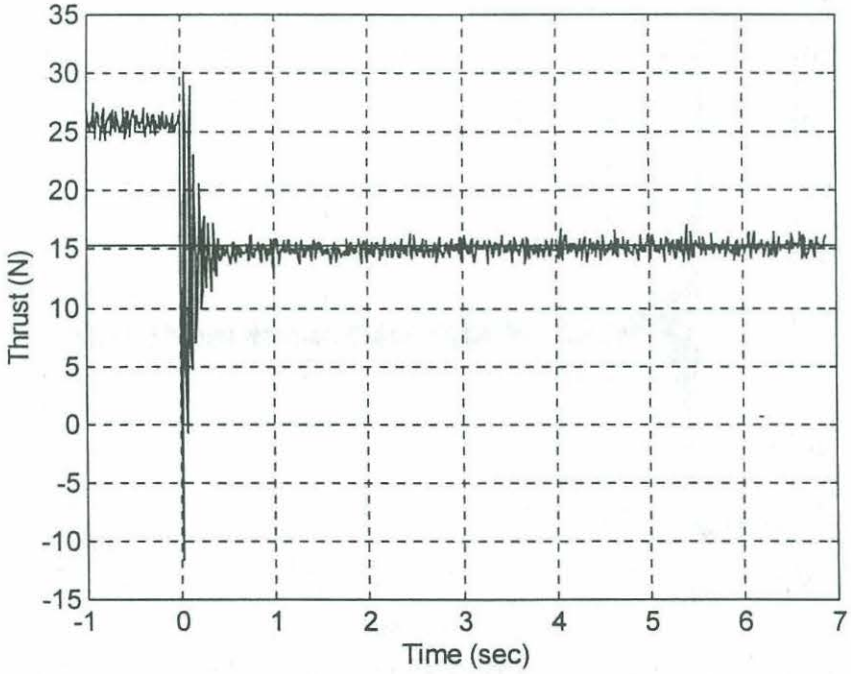

Figure 28: Thrust data for run 641.

undershoot of thrust.

5.9c Sinusoidal Perturbations

The effect of the soft test stand was reduced by using sinusoidal changes in velocity rather than step changes. These minimized the jerking of the test stand, keeping vibration to a minimum. This made the effect of a propeller undergoing maneuvering easier to see.

Run 615, plotted in figures 29 (velocity and torque) and 30 (thrust) was typical in many ways. This was a ductless run, with the impeller providing a flow of 0.24 m/s. An initial steady state condition was established with a shaft velocity of 40 rad/s. A sinusoidal perturbation of (+-) 12 rad/s with a period of 1 second was then added.

The torque and thrust data are plotted as solid lines with equivalent quasi-steady values plotted as dots for comparison. These values are what would have been obtained had the instantaneous shaft velocity been a steady state velocity. They were derived from fitting a spline curve of the values of thrust and torque obtained from the steady state runs described above, correlated to the instantaneous filtered velocity of the run being examined.

The behavior seen in the step changes is clearer in the sinusoidal perturbation run. As the propeller accelerates, it encounters a lower than normal inflow velocity and the resulting increased angle of attack results in a higher than normal thrust. As the propeller slows at the top of the perturbation and the local inflow at the propeller catches up, the thrust drops off as the angle of attack settles down. As the propeller slows during the downside of the perturbation, the angle of attack encountered is lower than

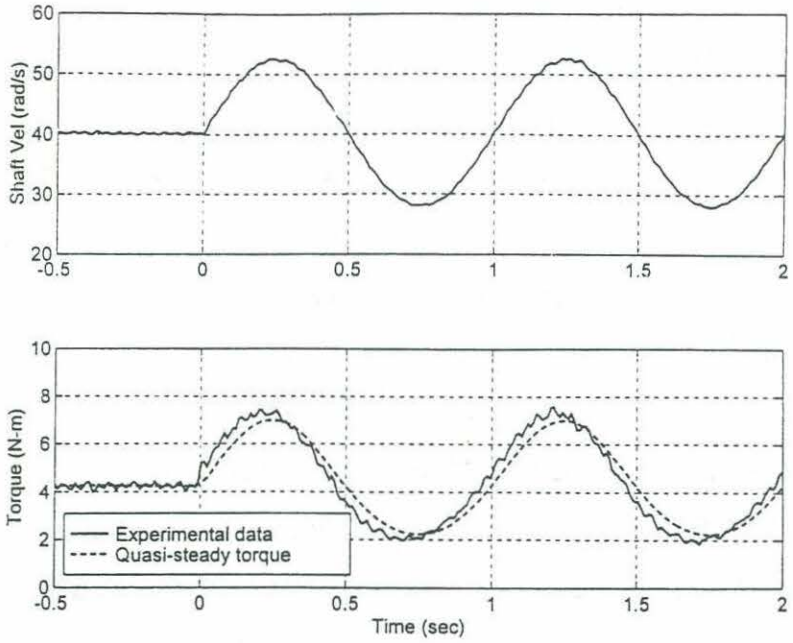

Figure 29: Velocity and torque data for run 615. Quasi-steady values are torque which would have been obtained had instantaneous velocity been steady state.

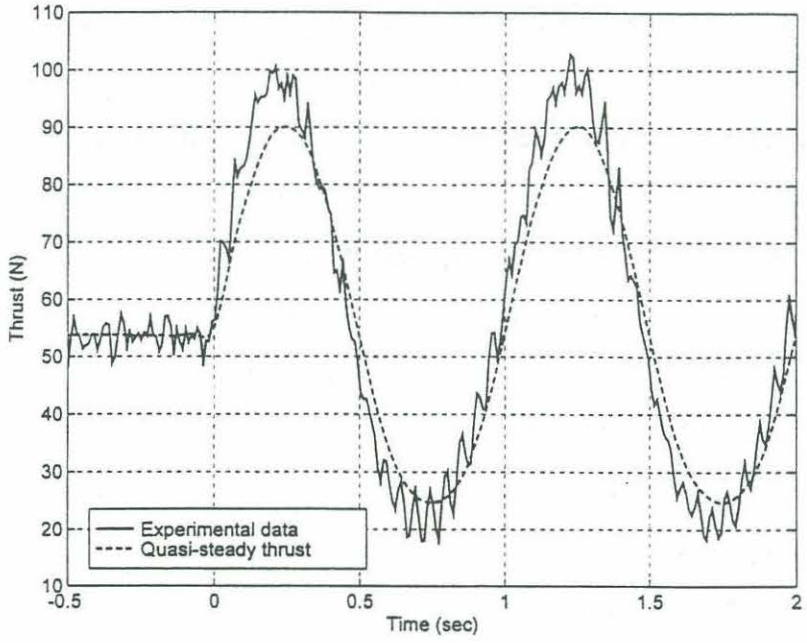

Figure 30: Thrust data for run 615. Quasi-steady values are thrust which would have been obtained had instantaneous velocity been steady state.

normal, and the thrust produced is lower than the quasi-steady result. The overall result is that the thrust seems to be leading the angular velocity.

Data from Run 672 is presented in figures 31 and 32. This was also a ducted run. The mean velocity was 40.5 rad/s (385 rpm) before the addition of a (+-) 12.5 rad/s (120 rpm) perturbation. The period was one second. These conditions are very close to the conditions of Run 615, except that in the case of run 672 the impeller was set for an inflow velocity of 0.514 m/s or one knot. This higher flow speed resulted in a general decrease in thrust.

Data from Run 673 is presented in figures 33 and 34. The operating conditions of this run were identical to run 672, except that in this case, the period was lengthened to 2 seconds. The result is that the acceleration of the propeller is less, so the angular velocity does not lead the fluid velocity as much and the amount of overshoot (and undershoot) is reduced.

Experimental runs that were made with the duct in place produced similar results. Run 315 data is presented in figures 35 and 36, while run 314 data is presented in figures 37 and 38. Both have an initial steady state velocity of 41.2 rad/s prior to a sinusoidal perturbation of (+-) 18.5 rad/sec. Flow velocity in both cases was 0.514 m/s. The difference in the two was the period of the perturbation, which was one second in run 315 and two seconds in run 314.

Several runs were done about a mean velocity of zero. This is a common situation for a vehicle in a hovering maneuver. A typical result of such a run is shown in figures 39 and 40. This was run 407, a ducted run with a perturbation of (+-) 50 rad/s (475 rpm). There

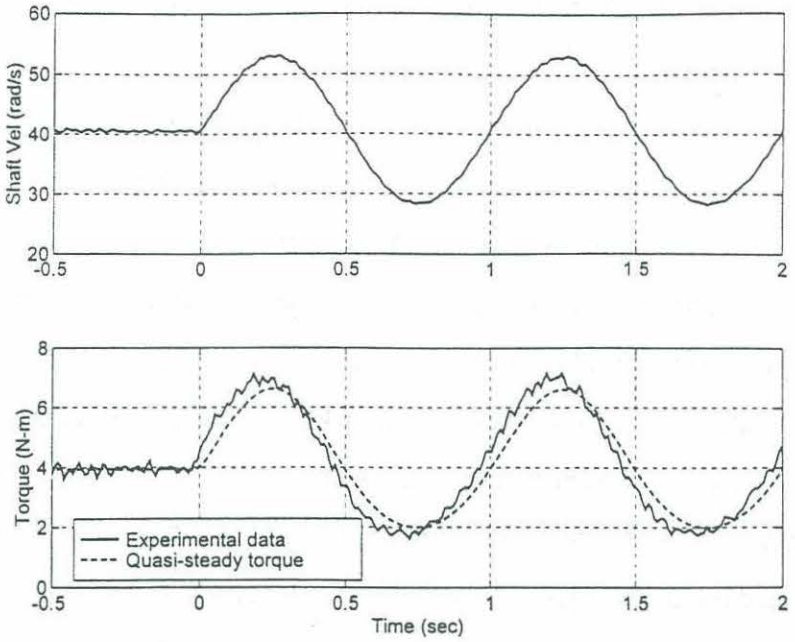

Figure 31: Velocity and torque data for run 672. Quasi-steady values are torque which would have been obtained had instantaneous velocity been steady state.

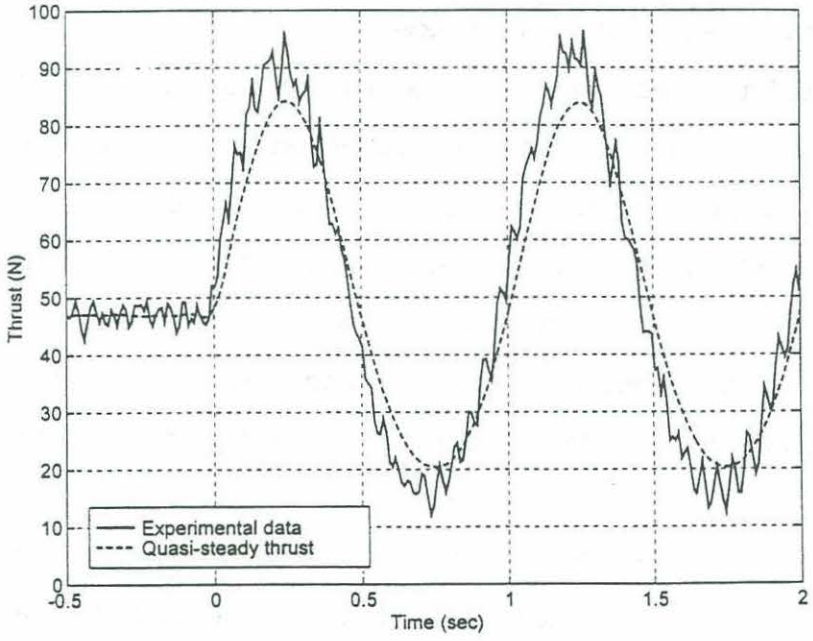

Figure 32: Thrust data for run 672. Quasi-steady values are thrust which would have been obtained had instantaneous velocity been steady state.

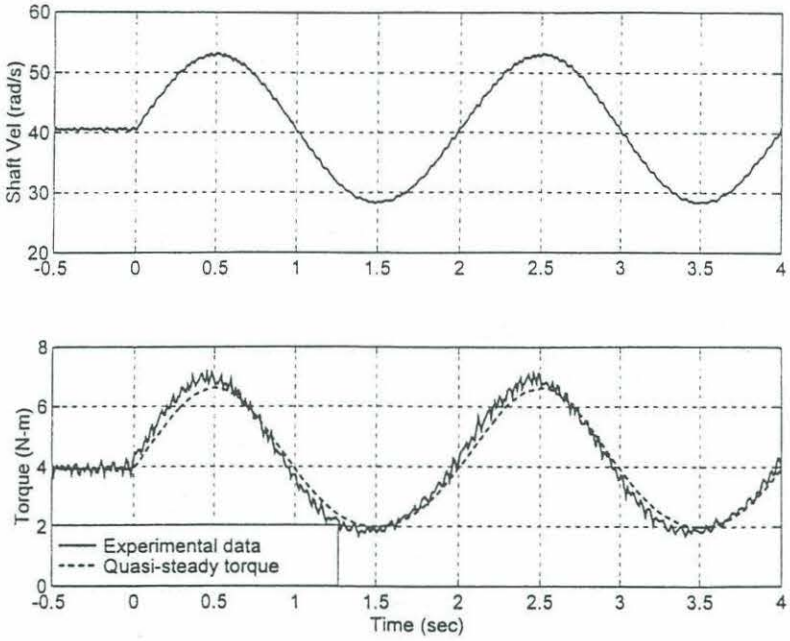

Figure 33: Velocity and torque data for run 673. Quasi-steady values are torque which would have been obtained had instantaneous velocity been steady state.

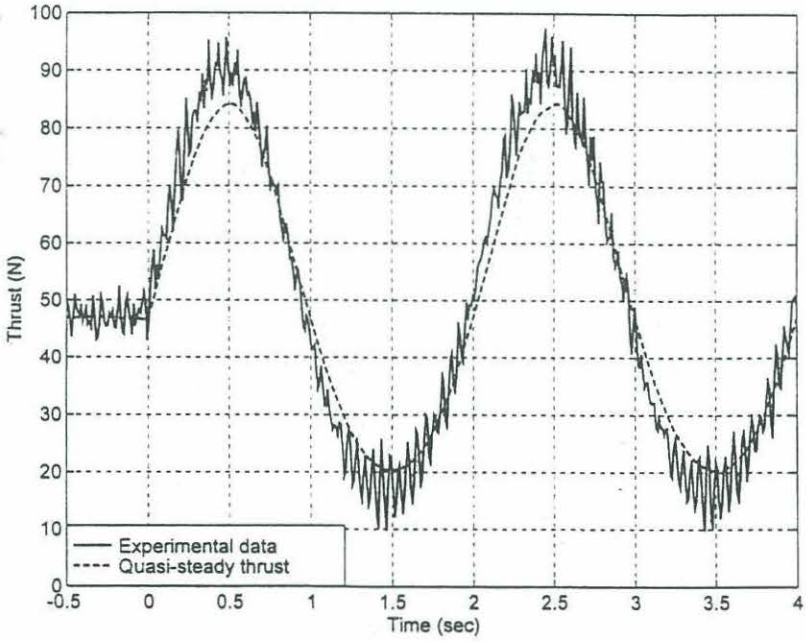

Figure 34: Thrust data for run 673. Quasi-steady values are thrust which would have been obtained had instantaneous velocity been steady state.

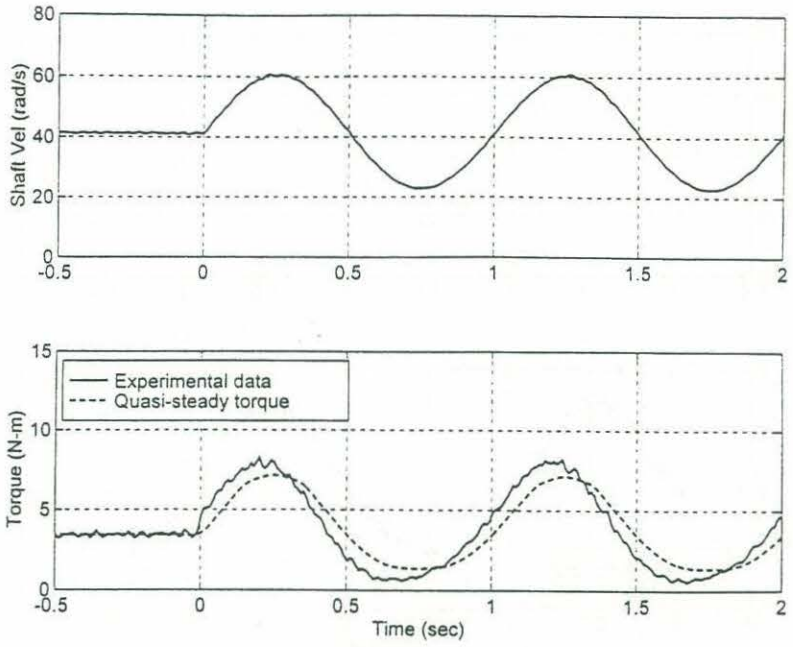

Figure 35: Velocity and torque data for run 315. Quasi-steady values are torque which would have been obtained had instantaneous velocity been steady state.

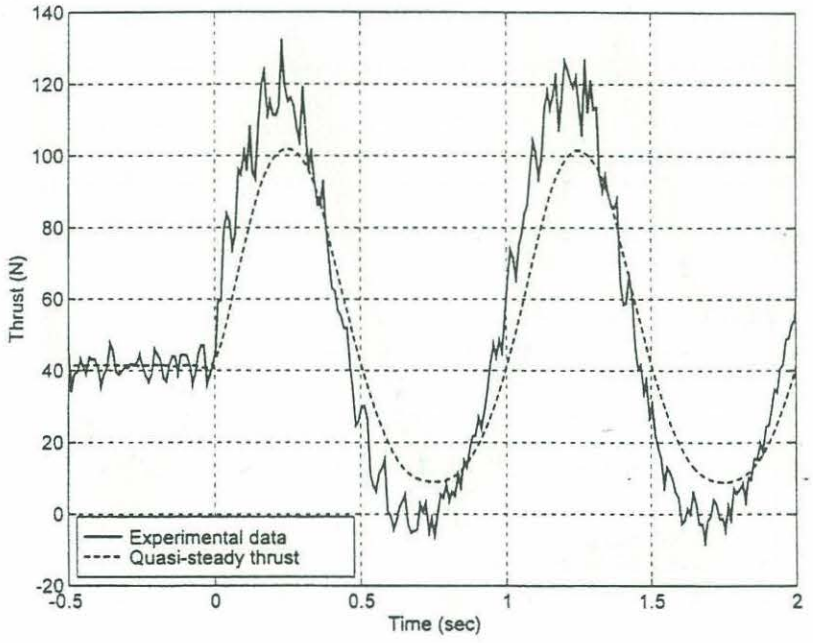

Figure 36: Thrust data for run 315. Quasi-steady values are thrust which would have been obtained had instantaneous velocity been steady state.

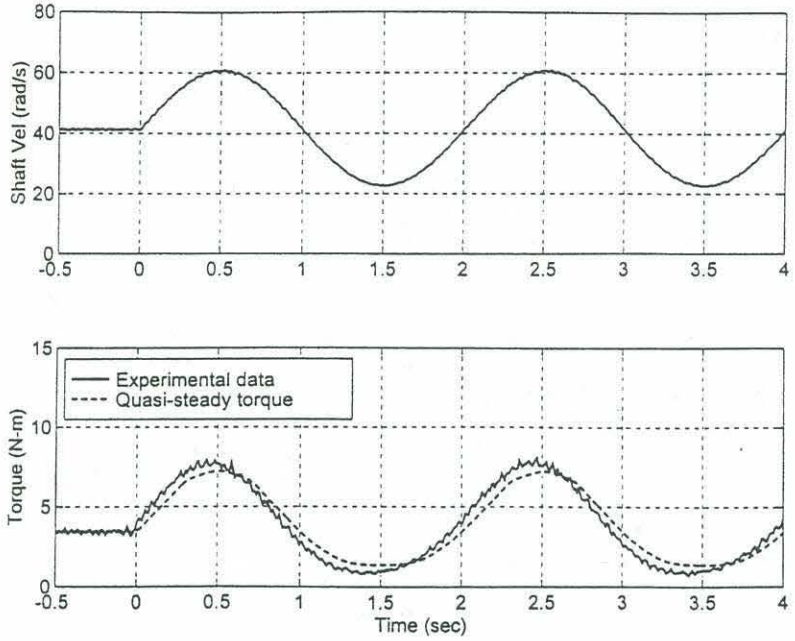

Figure 37: Velocity and torque data for run 314. Quasi-steady values are torque which would have been obtained had instantaneous velocity been steady state.

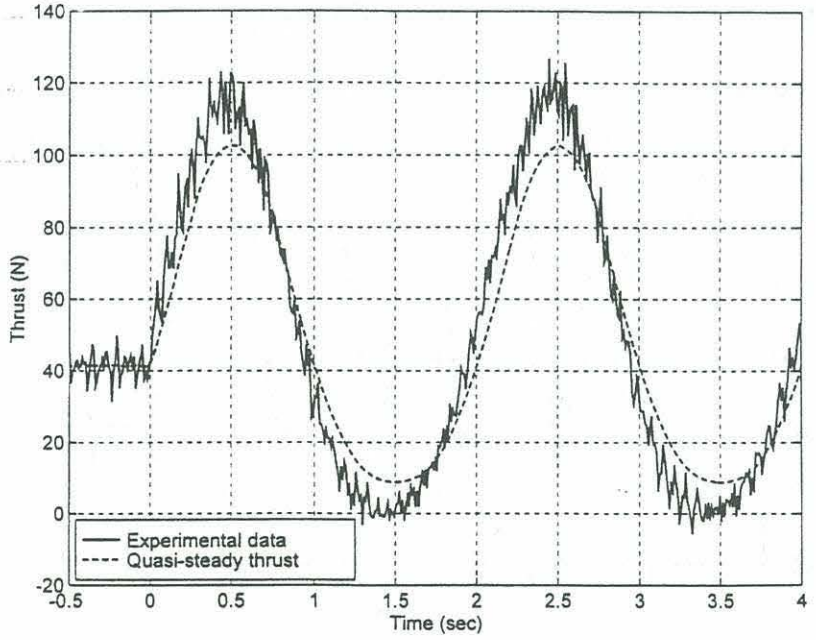

Figure 38: Thrust data for run 314. Quasi-steady values are thrust which would have been obtained had instantaneous velocity been steady state.

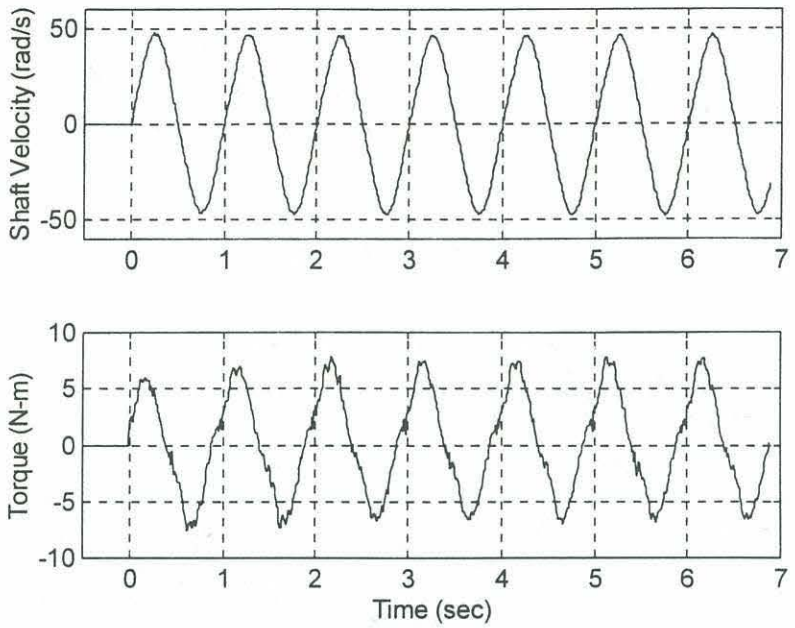

Figure 39: Velocity and torque data for run 407.

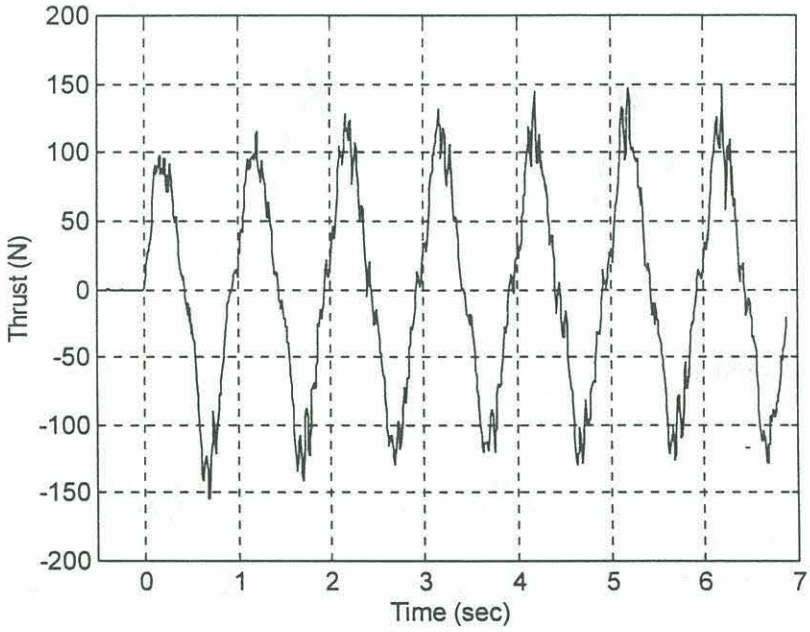

Figure 40: Thrust data for run 407.

are no quasi-steady values shown, since the impeller was turned off for these runs. Note that initially there is greater negative thrust than positive thrust, but that gradually it evens out.

Chapter VI Conclusion

6.1 Summary

The experimental results showed that a rapidly accelerating thruster will produce more thrust at a given advance coefficient than the same propulsor operating under the same conditions at steady state. This will result in an overshoot in commanded thrust. It was also shown that a rapidly decelerating propeller will undershoot the commanded thrust. It is clear that steady state propulsor performance is not applicable to estimating unsteady thruster operation. Improving the maneuvering control of underwater vehicles will require incorporation of these unsteady dynamics into the vehicle control algorithms.

The numerical simulation developed could not be used in the same range of advance coefficients as the experiments. Preliminary results showed behavior at high advance coefficients that was similar to the behavior observed in the experiments at low advance coefficients.

6.2 Recommendations for Further Study

To optimize the data obtained from future experiments, there are several areas which need to be addressed. Use of a different style of amplifier would reduce the noise produced which can be picked up by the data logging equipment. An amplifier that allowed more precise motor control than (+-) 0.3 rad/s (3 rpm) would reduce vibration. A

stiffer test stand is a must to be able to quantitatively determine the amount of overshoot. Whole field velocity data will become important as more work is done with fully reversing operations.

The numerical simulation program has a fair amount of evolvement to undergo before it is truly useful as a tool for studying and representing thrusters. In addition to solving the problems discussed earlier, the code should incorporate the possibility of a ducted propeller. Many of the vehicles that can benefit from this work use ducts or shrouds to protect the blades and improve thrust. This addition can rely on similar work with ducted propeller modeling for steady operation and nonuniform flows.

A complex leap for future work will be addressing the issue of reversing propellers. This is one area that has not been numerically modeled to my knowledge. The model developed to do this will need to deal with the propeller ingesting it's own wake, which is represented by singularities. In preparation for the task of modeling this event, it would be helpful to run experiments in which the entire flow field around the propeller is mapped, possibly through the use of Digital Particle Imaging Velocimetry. A thorough understanding of this process would greatly improve the control of underwater vehicles.

References

[1] Yoerger, D.R., Cooke, J.G., and Slotine, J.E., "The Influence of Thruster Dynamics on Underwater Vehicle Behavior and Their Incorporation Into Control System Design," IEEE *Journal of Oceanic Engineering*, Vol. 15, No. 3, pp. 167-178, 1990.

[2] Whitcomb, L.L., and Yoerger, D.R., "Comparative Experiments in the Dynamics and Model-Based Control of Marine Thrusters", IEEE Journal of Oceanic Engineering, submitted 1996.

[3] Healy, A.J., Rock, S.M., Cody, S., and Brown, J.P., "Toward an Improved Understanding of Thruster Dynamics for Underwater Vehicles," IEEE *Journal of Oceanic Engineering*, Vol. 20, No. 4, pp. 354-361, 1995.

[4] Lewis, E.V., "Principles of Naval Architecture," Vol. 2, pp. 131-145, Society of Naval Architects and Marine Engineers, Jersey City, N.J., 1988.

[5] Kerwin, J. E. "13.04 Lecture Notes: Hydrofoils and Propellers," unpublished, January, 1995.

[6] Saunders, H. E., "Hydrodynamics in Ship Design," Vol. 1, Society of Naval Architects and Marine Engineers, Jersey City, N.J., 1957.

[7] Kerwin, J.E., and Keenan, D.P., "Computational Aspects of Propulsor Design," Presented at the Marine Computers '91, Second Symposium on Computer Applications in the Marine Industry, Boston, September 1991.

[8] Greeley, D.S., and Kerwin, J.E., "Numerical Methods for Propeller Design and Analysis in Steady Flow," SNAME *Transactions*, Vol. 90, pp. 415-453, 1982.

[9] Kerwin, J. E., and Lee, C.S., "Prediction of Steady and Unsteady marine Propeller Performance by Numerical Lifting-Surface Theory," SNAME *Transactions*, Vol. 86, pp. 218-253, 1978.

[10] Keenan, D.P., "Marine Propellers in Unsteady Flow," PhD Thesis, Massachusetts Institute of Technology, Cambridge, Ma., May, 1989.

[11] Newman, J.N., "Marine Hydrodynamics", pp. 230-232, MIT Press, Cambridge, Massachusetts, 1992.

[12] Frydenlund, O., and Kerwin, J.E., "The Development of Numerical Methods for the Computation of Unsteady Propeller Forces," *Norwegian Maritime Research*, Vol. 5, No. 2, 1977.

[13] Lurie, Beth, personal communication, 1996.